Journal of South American Earth Sciences 119 (2022) 104017



Contents lists available at ScienceDirect

Journal of South American Earth Sciences

journal homepage: www.elsevier.com/locate/jsames





Environmental geology and isotopic evaluation of springs within the central part of the Sierra Cerro de La Silla, northeastern México

Jerjes Rigoberto Pantoja-Irys [a,*], Hugo Mujica-Sánchez [a], Luis Eduardo Arista-Cázares [b], César Michel Hernández-García [a], Mark Wagner [c]

[a] Corporación Ambiental de México S.A. de C.V. Texcoco 100, Colonia Satélite Acueducto, Monterrey, Nuevo León, 64960, Mexico
[b] Universidad Autónoma de Nuevo León, Facultad de Ciencias de La Tierra, Carretera a Cerro Prieto Km 8, Ex. Hacienda de Guadalupe, Linares, Nuevo León, 67700, Mexico
[c] Arcadis US, Inc. 7550 Teague Road, Suite 210, Hanover, MD, 21076, USA

ARTICLE INFO

Keywords:
Monterrey
Cerro de La Silla
Springs
Groundwater recharge
Isotopes
Geothermal reservoir
Rare earths
Aquifer
Sedimentary marine succession

ABSTRACT

The Monterrey Metropolitan Area (MMA), in the State of Nuevo León, México, has had a significant increase in its population and associated urban footprint for decades. From a population standpoint, it represents the second largest urban area in México. Its growth has required increasing infrastructure for the necessary services including public access to potable water, which will continue to increase over time. The supply of water resources for the metropolis comes mainly from groundwater sources. These sources are subject to certain conditions influenced by their geographical location, physiographical characteristics, and the geological environment, having a direct impact on the water recharge system of the regional aquifers. The government of the State of Nuevo León has developed an investment master plan for a water resource, outlined to be completed in 2050, which includes the construction of new dams and the setting up of additional shallow and deep production wells. With a constant annual population growth from one to five percent, additional stresses and vulnerability to this valuable resource will occur. Based on the changing demographics and additional stresses to water resources, it is essential to understand the localized natural groundwater regime extending from the precipitation recharge zones to the individual aquifers that serve the needs of the population. The following study evaluates specific aspects of the water regime (recharge zones and springs), in an area approximately 25 km south of central Monterrey, in the Santiago area of the MMA which is expected to have significant urban expansion in the future. The central portion of the Sierra del Cerro de la Silla, which constitutes the study area is a catchment and infiltration zone for meteoric water. Within the study area, five springs were identified and sampled during the dry season, and the collected spring water samples were submitted for geochemical and isotopic analyses. Field surveys, data collection and interpretation have contributed to the understanding of the water origin and associated physical-chemical characteristics during infiltration through the geological succession and ultimate incorporation into the aquifer. The characterization of the regime through a series of field surveys and the spring water characterization has determined the presence of a low enthalpy geothermal system at the depth, that has the potential to impact shallow freshwater regimes. In addition to contributing to the knowledge of the local hydrogeological system, this study can support the understanding of the vulnerability of the natural resource due to human activity and back up concepts of optimal use and protection.

1. Introduction

Groundwater is one of the fundamental sources of water supply for human consumption and other uses worldwide (Giordano, 2009). Population and urban growth demand a constant increase in the supply of water, which is causing ecosystems that depend on groundwater, directly or indirectly, to be increasingly threatened (Rohde et al., 2017). For this reason, the aquifers that currently supply large cities are overexploited, with recharge areas reduced and/or eliminated due to urbanization, causing the detriment of the quality of the water that infiltrates to the underlying aquifer systems. Water supply demand will continue to increase in urbanized areas with population growth.

* Corresponding author.
E-mail address: Jerjes.pantojai@anahuac.mx (J.R. Pantoja-Irys).

https://doi.org/10.1016/j.jsames.2022.104017
Received 18 June 2022; Received in revised form 29 August 2022; Accepted 29 August 2022
Available online 7 September 2022
0895-9811/© 2022 The Authors. Published by Elsevier Ltd. This is an open access article under the CC BY license (http://creativecommons.org/licenses/by/4.0/).

Ultimately, that will result in non-sustainable over-exploitation of the aquifers whereby extraction exceeds recharge, creating the need to seek mitigation actions and likely other sources of water. In addition, climate change has a significant effect on sustainable water supply, as extended periods of drought are occurring along with more intense short-term precipitation events which do not contribute to aquifer recharge. Sustainable groundwater supplies require both, a complete understanding of the groundwater regime including recharge conditions, and robust management plans to protect this valuable resource into the future. Mitigation measures that are often adopted also in México are 1) harvesting of rainwater for use during drought periods, 2) water recycling and re-use, 3) eliminating contaminant discharges that can impact soil and underlying groundwater, 4) creating "green areas" that are focused on enhancing aquifer recharge, and 5) promoting stormwater use and/or recharge to the aquifer system. These actions, individually or collectively, also require careful urban planning to protect the underlying water resources, to enhance recharge while protecting against degradation of water quality.

The city of Monterrey, capital of the State of Nuevo León is a prime example of urbanization with associated water stresses and risks. The city is part of a network of municipalities that make up the greater metropolitan area, which includes 12 municipalities with a population of more than 5.3 million inhabitants and a land area of 7657 km^2, making it the second largest metropolitan area in México (INEGI, 2020).

Thirty-eight percent of the drinking water supply for the Monterrey Metropolitan Area (MMA) comes from groundwater resources with 62 percent from surface sources. Surface sources include three dams: La Boca, Cerro Prieto, and El Cuchillo. Groundwater is extracted through a network of "shallow and deep" boreholes distributed in three main wellfields designated as "Topo Chico, Área Metropolitana, and Buenos Aires" (Aguilar-Barajas et al., 2021; Mora et al., 2017). The quality of the groundwater, extracted through wells located at the Sierra Madre Oriental (SMO), the Santiago municipality and Monterrey Valley, is of high quality (Mora et al., 2017).

Within the region there are a series of specific characteristics, typical of its geographical location, which contribute to its natural availability, as well as the quality of the water resource. The MMA extends at the foot of the Sierra Madre Oriental (SMO) mountain range, where the flat landscape of the great plain of northeastern México begins. The area is surrounded by mountains, foothills and rises in a relatively dry (semi-arid) with extreme climate environment, marking the transition zone (Aguilar-Barajas et al., 2021) between the coastal plain of the Gulf of México and the Chihuahuan Desert, the largest desert in North America (González and Sosa, 2003). The combination of these regional factors contributes to limited water availability; in the MMA it is further exacerbated by extensive urban sprawl with hardened surface. The precipitation is either lost due high evaporation rates, and stormwater runoff is directed to drainage systems and municipal sewers, significantly reducing infiltration to the subsoil to recharge underlying aquifers. The front fold and thrust belt of the SMO, which surrounds the metropolitan area serves as an excellent natural recharge zone for all of aquifers in the region as it occurs in the Cerro de La Silla Mountain range.

Many of the groundwater mitigation measures discussed above have been established within territorial directive planning, but water resource conditions remain highly stressed, and there are significant restrictions on receiving new water concession titles for groundwater or increasing the permitted volume of water use. As part of the overall mitigation efforts, a more in-depth understanding of the water cycle within the available water-bearing zones is critical. Aquifer vulnerability requires the assessment of the recharge zones, circulation patterns, and relative temporal transport to allow for more direct and detailed environmental planning to protect water resources. This paper focuses on the Cerro de La Silla Mountain range water resource recharge zones and springs, and the research that was conducted contributes to the understanding of the water cycle conditions and environmental vulnerability.

The Cerro de La Silla Mountain range is a protected natural area, which due to its geological characteristics, constitutes a catchment area as well as a filtration area for meteoric water. Countless springs and seeps emanate throughout the length and breadth of this mountainous system. Protected natural areas were created aiming at the preservation of their natural resources and have become a natural laboratory to study their different components (González and Sosa, 2003). Accordingly, springs are, in most cases, the only natural access point to water, to develop a deeper understanding of physical-chemical conditions of recharge zones and groundwater within the aquifer system. They also allow for the understanding of the interaction between groundwater and the geological framework of the environment, including its mineralization and chemical evolution in time and space (Albert et al., 1979).

For this study, the rationale for the selection of the springs of the Cerro de La Silla Mountain range central portion (SCScp) was to establish a deeper understanding of the environmental geology and water dynamics of rainwater (Fig. 1), infiltration recharge in the high mountains, the regional aquifers, and the deeper water-bearing zones with unique characteristics. Specific rationale for selecting the study area include: 1) perennial springs arising in the upper, intermediate and lower portions of the mountain range both to the east and west, thus providing geochemical and isotopic data of the groundwater as it flows through the mountain; 2) the ecosystem in the central portion of the mountain has not been significantly disturbed; and 3) the singular presence of the El Bañito thermal spring (mEB) that provides valuable information on the natural processes that occur at greater depths, allowing for an indirect inference of the lithologies that do not emerge in outcrops but underlie the mountain range, among other relevant data.

2. Methodology

During 2021, field and desktop activities were performed to generate the information contained in this investigation. The different thematic maps, their calculations and the geological sections were developed using a digital elevation model (DEM) with a LiDAR (*Light Detection and Ranging*) resolution of five (5) meters (m), obtained from INEGI (2012) with a scale of 1:10,000 and digitized via ArcGIS Pro 2.6.0. Fracture, fault, and strike rosettes were plotted with the Faultkin program, version 8, and plots with Veusz, 3.2.1 version. The stratigraphic sections measured in the field were performed using staff-mounted Garmin model GPSMAP 64sx equipment with the Garmin GLONASS antenna, tape and compass. A DJI Mavic 2 Pro drone was also used to observe geological outcrops in places with difficult access. The petrography of the sedimentary rocks was described with the use of an Olympus model BX53M polarized microscope. Thin sections of rock samples were classified using Dunham (1962) and Folk (1962).

For groundwater that emerges from the SCScp springs, electrical conductivty, total dissolved solids, salinity, dissolved oxygen, hydrogen potential, redox potential and water temperature were measured with a YSI Professional Plus model W14S digital probe. Ambient temperature was measured with a Steren model TER-150 digital thermometer, and water turbidity was measured using a Hanna Instruments Model 93703 digital turbidimeter. These digital equipments were calibrated following the manufacturer's recommendations.

Groundwater samples from each spring were collected in two 1-L, 0.250-L plastic bottles with Teflon caps, which were submitted for geochemical and isotopic analysis to the Activation Laboratories Ltd. (Actlabs) laboratory located in Ancaster, Ontario, Canada (https://actlabs.com). The protocols for temperature (<4 °C) and preservation of the samples were followed according to the guideline of the analytical methods utilized. The collection of groundwater samples from the five springs for shipment to the laboratory was performed on January 31 and February 2, 2021, representing the dry season, after eight (8) days of moderate winter rain. Table 1 includes the analytical methods used for the detection of different parameters in the spring water samples.

From the analytical results, a multidimensional classification was

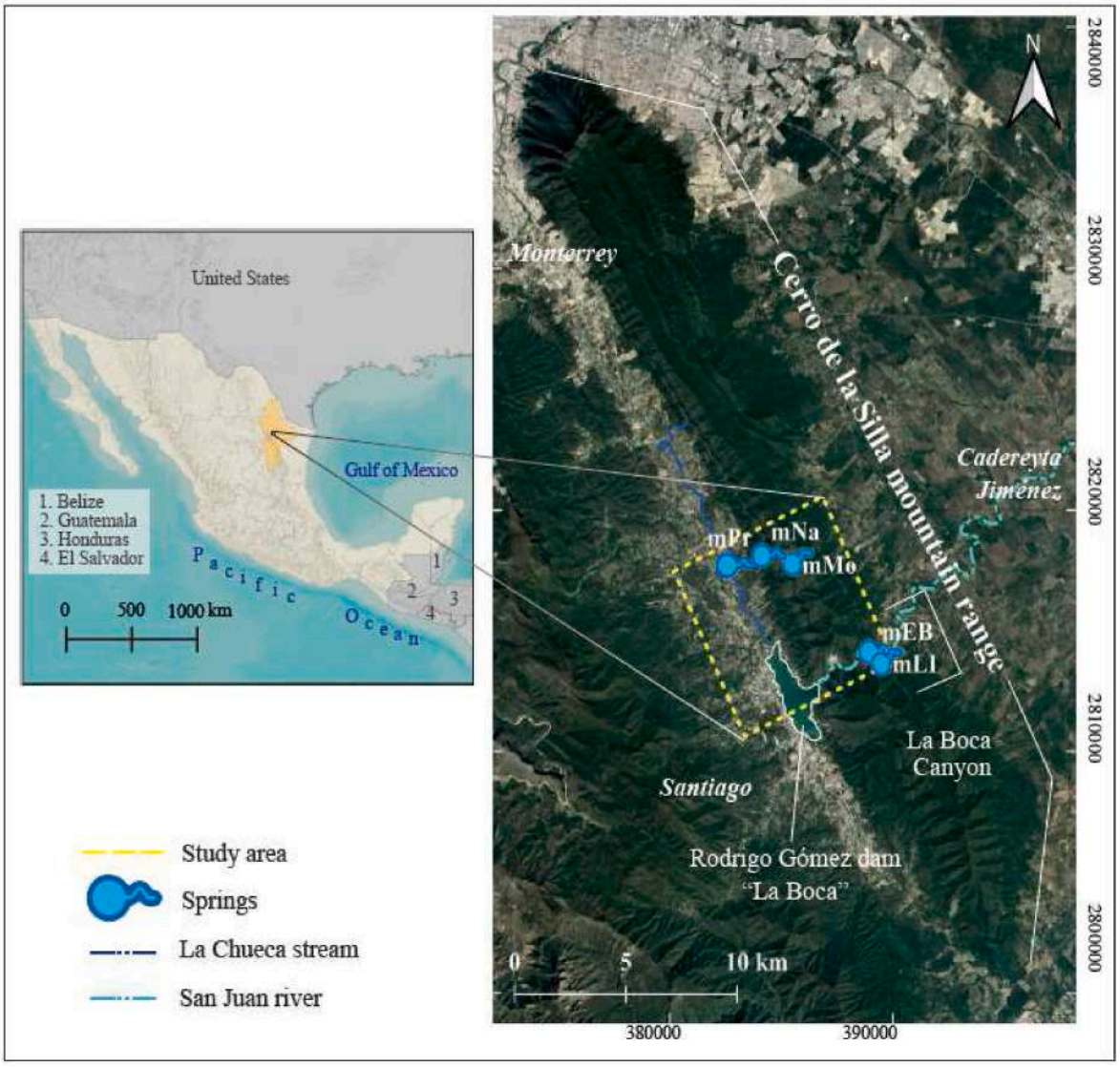

Fig. 1. Location of the research area and emergence of the SCScp springs in northeastern México. Where mPr = Princess spring; mNA = Naranjos spring; mMo = Montegrande spring; mEB = El Bañito spring; and mLI = La Ilusión spring.

Table 1
Analytical methods and specifications.

Laboratory Code	Parameters	Specifications
Code E6MB-ICP-MS	Trace elements, cations and rare earths.	Perkin Elmer Sciex ELAN 9000 ICP-MS, Perkin Elmer Nexion, Thermo icapQ o Agilent 7700.
Code E6B-Anions	F, Cl, NO_2, NO_3, PO_4, Br, SO_4	DIONEX DX-120 Ion Chromatography System
Code E6C-Alkalinity	$CaCO_3$, HCO_3 y CO_3, OH	Titration with glass pipette.
Code E6C-Silica	SiO_2	ICP-OES Varian Vista 735 ICP
Code 10A-18O	Isotope $\delta^{18}O$	Cavity Ring-Down Spectroscopy (CRDS)
Code 10A-Deuterium	Isotope $\delta^{2}H$	CRDS (Model L2130-i) (Picarro, California, USA).
Code 10A-$^{87}Sr/^{86}Sr$	Isotope ^{87}Sr and ^{86}Sr	Thermal Ionization Mass Spectrometry (TIMS), TI-Box, spectromat, Germany

generated using the *Water Molar Classification System from Linear Discriminant Analysis* computer program (Verma et al., 2021). The saturation index (SI), the speciation compounds and the geothermometric modeling were calculated using the PHREEQC version 3 geochemical package (Parkhurst and Appelo, 2013). For data entry, the concentrations were expressed in the same unit of measurement (mg/l), the dissolved oxygen value was converted from a percentage to mg/l, the reduction oxide potential in mV was then expressed in Eh values in V, and finally transformed to *pe* values that were entered to establish the redox conditions.

In this work multiple geothermometers were calculated using the SolGeo package (Verma et al., 2008) or direct calculation using the equations proposed by Blasco et al. (2018). It is important to mention that in the El Bañito thermal spring and its surroundings, large fumaroles that allow effective gas sampling were not observable with the naked eye; therefore they were not included in the sampling plan.

3. Description of study area

The Cerro de La Silla Mountain range exposes one of the last NW-SE folds of the Flanco Oriental (Eastern Flank) subprovince within the Sierra Madre Oriental province (Lugo-Hubp, 1990); and it has been morphoclimatically classified as a fossil or inactive karst of folded and faulted mountains (Espinasa-Pereña and Nieto-Torres, 2015). It represents an important recharge zone for the Huajuco canyon aquifer in the

State of Nuevo León. The National Water Commission (CONAGUA, 2020) considers that this aquifer is made up in its upper portion by alluvial and foothill sediments of varied granulometry, resulting from the weathering of pre-existing rocks and polymictic conglomerates that fill the valleys, especially within the bed and below the La Chueca stream. The lower portion of the aquifer exists in a fractured medium made up of clayey limestone and calcareous shale. The boundaries and barriers to the groundwater flow, as well as the hydrogeological basement, are represented by the same clay-calcareous succession where the fracturing disappears, preventing the water from flowing at depth. At greater depths, the limestones constitute the deep aquifer systems that present secondary permeability as a result resulting of fracturing and dissolution, and the presence of semi-confined and confined conditions, due to the fact that they are underlain and overlain by an alternation of shales and siltstones. The piezometric level of this aquifer is very shallow on the banks of the La Chueca stream, but gradually increases as the slope of the mountain range increases.

The topographical relief of the SCScp presents three general behaviors: 1) a watershed whose levels and slopes soften towards the east and west from an elongated NW-SE ridge; 2) steep slopes from NE-SW and N–S crests; and 3) steep slopes greater than 45°, that cut the entire sedimentary succession with NE-SW and N–S trends in the La Boca canyon. The highest topographic point in the study area has an elevation of 1151 m a.s.l., while the lowest elevation is 388 m a.s.l. Stormwater drains, in this portion of the mountain range, to the east and west following the first-order stream channels that have formed in a NE-SW and N–S direction; with NW-SE tributaries. These streams are not perennial and only carry water during heavy rain events. The La Chueca stream marks the origin of the water system (base) of the Río Grande (*Río Bravo*)-San Juan basin (CONAGUA, 2020). This stream is perennial and runs parallel to the crest of the mountain range in the west until it reaches the Rodrigo Gómez dam (La Boca); whose waters flow through the La Boca canyon with a NE-SW and N–S direction, continuing in a smooth and undulating channel in the Gulf Plain, feeding the San Juan River, which run into the Rio Bravo.

The weather stations La Boca (code 19–069) and Santiago (code 19–065), of the National Meteorological Service (SMN, 2021), have recorded an average annual temperature of 21.3 °C, with a maximum temperature of 45.5 °C and a minimum of −7.0 °C. The total annual precipitation varies from 1001 to 1124 mm, with greater intensity towards the southwest of the mountain range. The months of September and August have the highest rainfall totals and December, the lowest recorded value. Aguilar-Vásquez (2003) determined two main types of vegetation in the mountain range, with topographic elevation analysis in a GIS model, having submontane scrub in the lower areas (600–800 m a.s.l.) and oak forest at the higher elevations (800–1000 m a.s.l.). At the time the state protected natural area was regulated, 285 species of vascular plants had been registered, as well as 173 species of vertebrates, of which 19 were included in the official Mexican standard NOM-059-SEMARNAT-2010 (SEMARNAT, 2010).

3.1. Springs of the central portion of the sierra Cerro de La Silla

The Montegrande (mMo, 610 m a.s.l.) and Naranjos (mNa, 525 m a.s.l.) springs arise on the eastern slope of the SCScp, the Princess spring (mPr, 488 m a.s.l.) on the eastern margin of the Huajuco canyon, the El Bañito thermal spring (mEB, 405 m a.s.l.), and La Ilusión (392 m a.s.l.) in the La Boca canyon on the eastern flank of the mountain range (Table 2). Although there are more non-thermal springs in the SCScp, these were selected for evaluation because they present a constant and quantifiable flow in the upwelling zone, they are at different altitudes, they arise in different geological formations, and they are accessible. These facts facilitate contrasting and thus better understanding of their characteristics as a mountainous hydrogeological system. It should be noted that the authors did not find geological, geochemical or isotopic references associated with any of the springs in the public record; so the genesis of the thermal spring has not been previously defined.

Table 2
Location and use of springs.

Spring	Coordinates UTM/ WGS 84 (m)		Altitude (m a.s.l.)	Flow (l/s)	Use
Montegrande	0385460	2817755	610	~0.125	Natural
Naranjos	0384192	2818184	525	~0.166	Water Supply
Princess	0382671	2817795	488	~0.315	Recreational
El Bañito	0389167	2814032	405	~1.266	Recreational
La Ilusión	0389510	2813652	392	~0.591	Natural

The mMo arises in the upper mountainous part in its north-central portion (Fig. 2A); it has a low flow rate of 0.125 l/s as measured in the dry season, in very coarse folded strata (>1.2 m) of radiolarian wackestone-textured limestone and calpionellids, with load-bearing surfaces, diagenetic stylolites, occasional flint nodules, and recent travertine deposits. The mNa arises in the intermediate part of the mountain range in its north-central portion (Fig. 2B). It has a measured dry season low flow of 0.166 l/s, in folded strata of limestone having a wackestone texture with radiolaria and foraminifera in thicknesses ranging from very thick to thin, with undulating surfaces, abundant organic matter, and medium bands of flint. The mLI, at the lowest altitude (Fig. 2D), arises in the southern portion. It has a measured moderate dry season flow of 0.591 l/s, in very coarse folded strata (>1 m) made up of a calcareous breccia of sub-angular clasts up to 0.5 m, poorly classified, alternating with very coarse limestone stages (<1 m) of wackestone texture with radiolaria and other microfossils, load-bearing surfaces and diagenetic stylolites. These three springs have been classified as draining (Jordana et al., 2009); that is, they are springs that drain a perched aquifer, where the emerging level is below the average saturation level, so they act as a bottom drain.

The mPr emerges on the western side of the La Chueca River in the northern portion (Fig. 2C). It has a moderate measured dry season flow of 0.315 l/s, in very coarse strata (>1 m) made of calcareous foliated shale with a mudstone texture with few reworked microfossils, organic matter and opaque minerals. Currently, the periphery of the spring is covered by soil and grass as it is used for recreational purposes. This spring has been classified as emerging (Jordana et al., 2009); that is, it is a spring that drains from an aquifer whose maximum saturated thickness is below the emergent level and acts as a spillway. Unlike the drains, if the spring stops providing water, the aquifer could continue to be exploited below the emergent level. The mEB is the only known thermal spring in the Cerro de La Silla Mountain range (Fig. 2E), arising in the southern portion of the study area with a flow rate of 1266 l/s, in very coarse folded strata (>1 m) made of calcareous shale foliated with abundant organic matter and thin bands of bituminous shale. It has been classified as phyllonian (Jordana et al., 2009) as it is representative of a "deep circuit", but it is in sedimentary rocks. This thermal spring is located within the CD2-SMOr Sierra Madre Oriental geothermal province (Prol-Ledesma and Morán-Zenteno, 2019). The province is dominated by thermal conductive effects, with heat fluxes increasing towards the west, and the average temperature of hydrothermal manifestations is around 45 °C.

Based on the geological survey carried out in this study (Figs. 3 and 4), it was defined that the mMo arises in the intermediate portion of the San Ángel Formation; the mNa arises in the Cuesta del Cura Formation, it is very close to the contact with the Agua Nueva Formation; the mPr arises in the lower portion of the Méndez Formation; the mEB arises in the middle-upper portion of the La Casita Formation; and the mLI arises at the base of the La Casita Formation in the thrust area. Each of these formations is described in detail below.



Fig. 2. Photographs of SCScp springs in northeastern México. A) Montegrande, B) Naranjos, C) Princess, D) La Ilusión, and E) El Bañito. 1.2 m graduated staff in 0.2 m segments and 0.33 m geologist's hammer.

4. Geology

4.1. Regional

An Andean-type subduction zone with the Farallon plate was established along the paleo-Pacific margin during Early Jurassic time (Ocampo Díaz et al., 2019). During the Toarcian (latest Early Jurassic), the subduction slab migrated from west to east towards the Yucatan block (Ocampo-Díaz, 2011; Ocampo Díaz et al., 2019, Fig. 1). This resulted in the emplacement of rhyolite, rhyodacite, dacite and andesite of the Nazas and La Boca formations at ca. 190−170 Ma, as documented by magmatic zircon (Fastovsky et al., 2005; Barboza-Gudiño et al., 2008; Rubio-Cisneros and Lawton, 2011; Lawton and Molina-Garza, 2014) on the Precambrian basement of eastern and northeastern México. A continental and marginal-marine sedimentary system developed in intra-arc, back-arc, extensional and transtensional continental arc basin settings. The continental La Boca, La Joya, and Todos Santos formations, as well as the deep-marine siliciclastic Huayacocotla Formation were deposited by these systems (Barboza-Gudiño et al., 2008,2014; Venegas-Rodríguez et al., 2009; Godínez-Urban et al., 2011a; Rubio--Cisneros and Lawton, 2011; Ocampo-Díaz, 2011; Ocampo-Díaz and Rubio-Cisneros, 2013). The sedimentary system was fed by detritus from Triassic and older rocks (Venegas-Rodríguez et al., 2009; Godínez-Urban et al., 2011a; Rubio-Cisneros and Lawton, 2011). The roll-back of the paleo-Pacific slab of the Farallon plate not only triggered the migration of the continental Nazas magmatic arc and the mantle asthenospheric flow but also favored crustal thinning of the overriding Guerrero plate. This caused exhumation of the Early Jurassic volcanic rocks and older metamorphic basement rocks in an extensional and transtensional continental arc basin during the Middle Jurassic

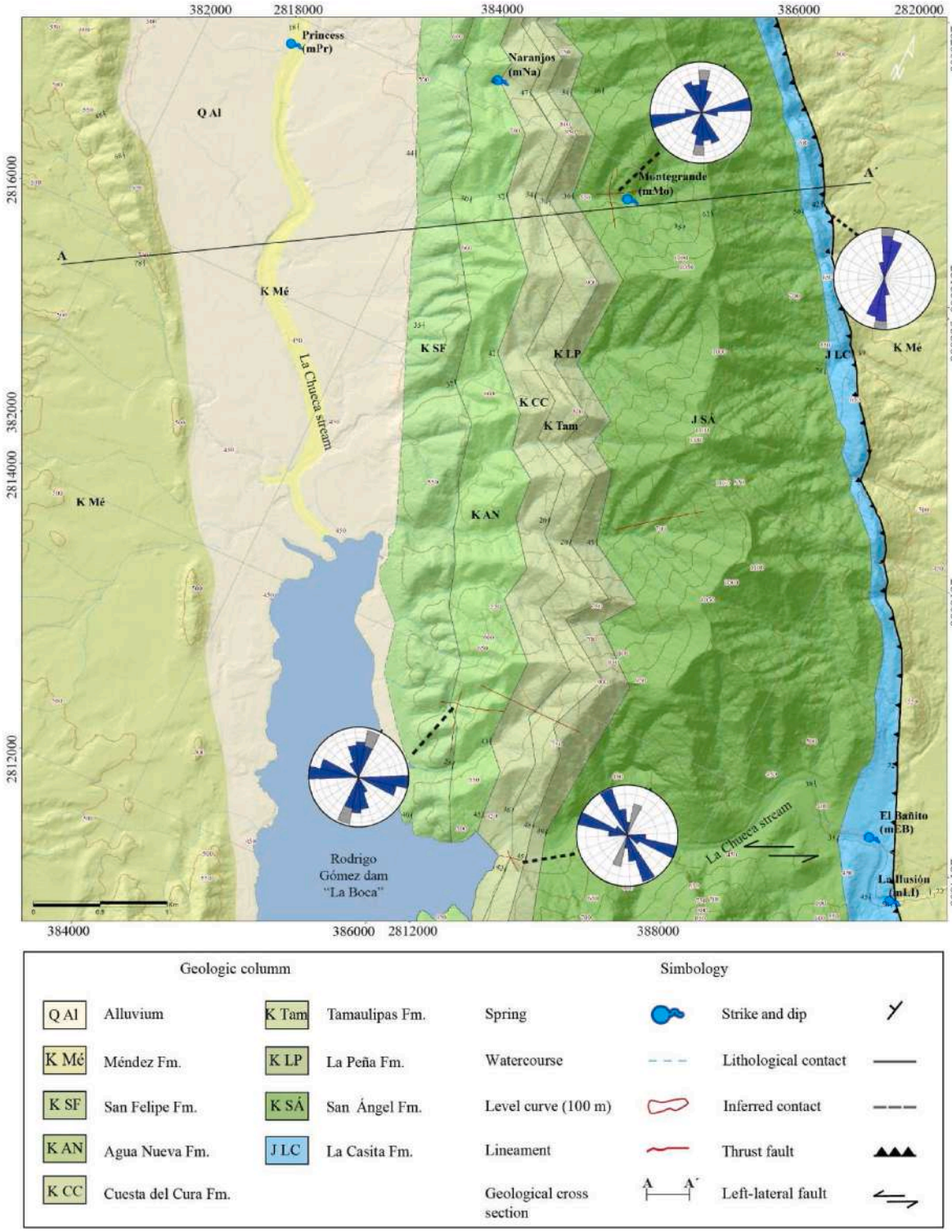

Fig. 3. Geological map of the SCScp and location of the investigated springs.

(Ocampo-Díaz, 2011; Rubio-Cisneros and Lawton, 2011; Ocampo-Díaz and Rubio-Cisneros, 2013; Ocampo Díaz et al., 2019, Fig. 1C). Meanwhile, the initiation of western Pangea breakup led to the counterclockwise rotation of the Yucatan block on the Atlantic margin side (Pindell, 1985; Dickinson and Lawton, 2001; Pindell and Kennan, 2009; Godínez-Urban et al., 2011). This caused the development of horst-and-graben systems at the margin of the Gulf of México, as well as continental evaporite sedimentation (Marton, 1995; Dickinson and Lawton, 2001; Fillon, 2007). During the Late Jurassic, changes in the subduction angle of the Farallon plate underneath the Guerrero plate evolved into a high-angle oblique subduction zone that also developed an extensional and transtensional continental arc (s.s., Busby, 2012). The arc was associated with normal and lateral faults that favored exhumation and erosion of the Early to Middle Jurassic volcano-sedimentary successions of the Nazas arc (Bassett and Busby, 2005; Ocampo-Díaz, 2011; Ocampo-Díaz and Rubio-Cisneros, 2013; Barboza-Gudiño et al., 2015; Centeno-García, 2017; Ocampo Díaz et al., 2019, Fig. 1C). During the Late Jurassic, the continued opening of the

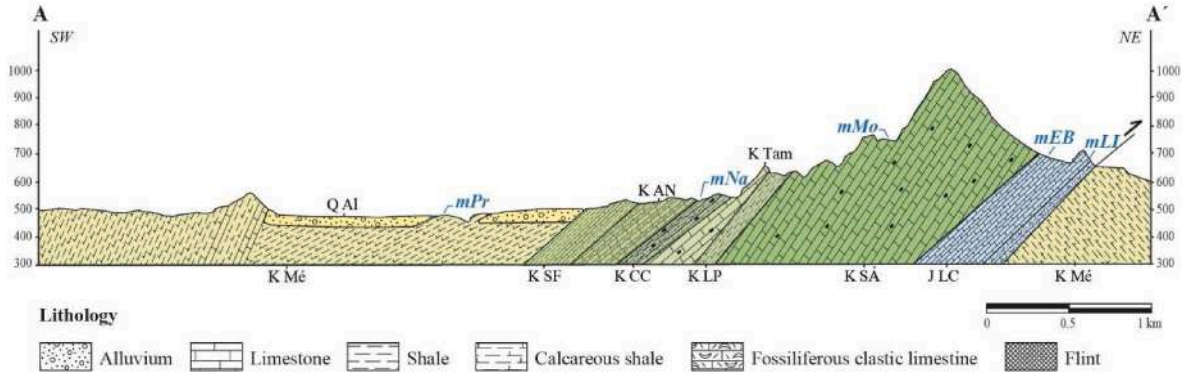

Fig. 4. Stratigraphic Section A-A′(see Fig. 3 for location and nomenclature).

Gulf of México led to left-lateral strike-slip faults, pull–apart and strike-slip basins in México and southern USA (e.g., the Chihuahua and Monterrey troughs; Rosaz, 1989; Goldhammer, 1999; Haenggi, 2002; Bassett and Busby, 2005; Ocampo-Díaz, 2011). Subsequent detachment of the Yucatan Block is linked to the Tehuantepec fault. It caused: a) intense counter-clockwise rotation of 10° of the Yucatan block (Molina-Garza et al., 1992; Pindell and Kennan, 2009), b) normal faulting of tectonic assemblages at the fringe of the uplifted blocks, and c)



Fig. 5. *Panoramic Photographs of the research area. A) Eastern slope in the north of the SCScp; B) La Boca Canyon; and C) Western Slope in the south of the SCScp.*

continued deposition of continental evaporites in the same area (Marton, 1995; Alaníz-Alvarez et al., 1996; Pindell and Kennan, 2009). Due to the Gulf opening, the Tethys Ocean flooded the continent from the east. This favored peritidal carbonate deposition on the transgressive clastic coastlines (e.g., Michalzik and Shumman, 1994; Ocampo-Díaz, 2011; Ocampo-Díaz et al., 2014; Ocampo Díaz et al., 2019, Fig. 1C). The Jurassic-Cretaceous boundary and Early Cretaceous time were characterized by abrupt changes in sedimentation from clastic to carbonate, a climatic shift from semi-arid to humid tropical conditions, as well as changes in chemical, biotic and tectonic conditions (cf., Adatte et al., 1996; White et al., 2005). The changes were a result of the opened Gulf of México and the reactivation of the continental magmatic arcs at the north-western and south-western parts of the paleo-Pacific margin (García-Díaz, 2004; Ocampo-Díaz, 2011). During the Early Cretaceous, the continued rotation of the Yucatan block caused the development of large carbonate platforms on basement highs (e.g., Coahuila, Valles-San Luis Potosí and El Doctor platforms), as well as marginal-marine clastic systems (Winker and Buffler, 1988; Pindell and Kennan, 2009; Ocampo-Díaz, 2011). Simultaneously, the Farallon-plate subduction below the Guerrero plate caused the development of a new continental arc related to the Alisitos-Guerrero subduction system in the southwestern USA and southern México (Boschman et al., 2018). In central México a left-lateral transform-fault related continental margin formed. It caused the subduction zone to migrate from northern to southern México (Ocampo-Díaz, 2011; Ocampo-Díaz et al., 2014).

4.2. Local

The Cerro de La Silla Mountain range has been structurally described and represented by several authors (Tardy et al., 1975; Longoria and Dávila, 1979; Olivares-Ramos, 2006; and Romo-Ramírez et al., 2021), through maps and sections, as a recumbent anticline to the east with a NW-SE orientation, ~20 km long by ~7.5 km wide, an altitude of up to 1800 m a.s.l., with its semi-domic north end and near symmetric south end. The central part, on its eastern slope (Fig. 5A), presents a distinctive feature as a thrust occurs that is truncated to the south by a left lateral fault, which contributes to the formation of the La Boca canyon (Fig. 5B) dissecting the mountain range in its central portion. It is in this central portion, on the eastern and western slopes, where the evaluated springs arise (Fig. 5C).

The anticline has been formed in a powerful sedimentary succession, located in the extreme northeast of the Late Cretaceous-Eocene Mexican Orogeny (Fitz-Díaz et al., 2018). Gray et al. (2001) consider that the "new" foreland basin was formed from the fold and thrust front with deep burial that reached up to 7 km thick, in this northern region, beginning at the same time as the orogeny and culminating shortly after that it had stopped. The lifting of this sedimentary succession began approximately 30 million years ago, and a large part of the sediments that covered it in the Paleogene have been eroded.

The oldest rocks that outcrop in the SCScp are found in the foothills of the eastern slope of the mountain range (Fig. 6); they are considered to be from the Upper Jurassic of the La Casita Formation. These rocks are found overriding younger rocks of the Mendez Formation. From this structure, the exposed stratigraphical formations transitionally become younger from east to west, having a thickness of 3378 m of this succession in the study area. It should be noted that the entire thickness of the sedimentary basin in the SCScp is even greater, since the lower part is not exposed due to the thrust, and the upper part continues west beyond the western limit of the study area. Below is a description of the stratigraphic formations that outcrop in the SCScp.

4.2.1. La Casita Formation

The first description of this lithological unit was made by Imlay (1936) in the La Casita canyon in the sierra de Parras in in the State of Coahuila. For this stratotype, a basal and slope environment in deep waters is proposed, during the Kimmeridgian and lower part of the

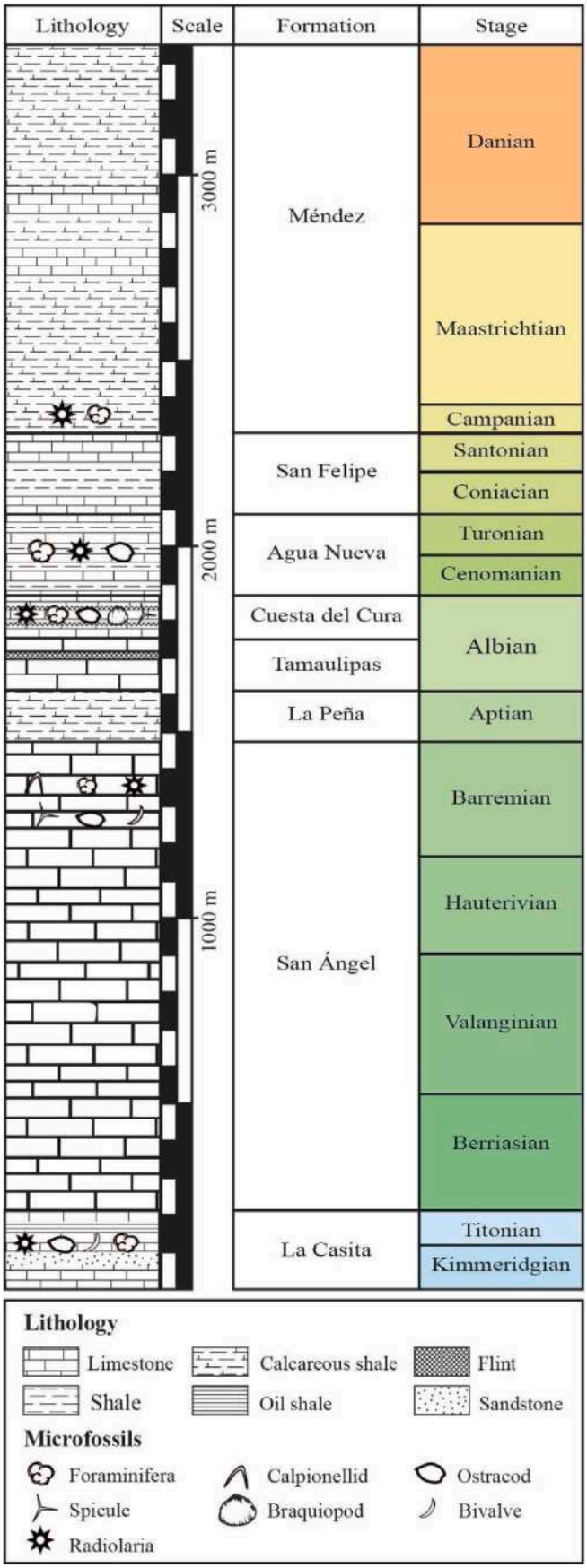

Fig. 6. Stratigraphic column of the sedimentary succession that outcrops in the SCScp (modified from Longoria and Dávila, 1979).

upper Tithonian, having a thickness of 107 m.

In the study area, the La Casita Formation has a minimum thickness of 135 m in the north, and a maximum thickness of 211 m in the south; it is exposed in 2.60% of the investigated area, and it is exposed between elevations ranging from 394 to 748 m a.s.l., on the eastern slope of the mountain range. The fold of this formation has a measured NW 50°-74° SE strike with dips of 32° to 48° SW.

The first strata that overlie the Méndez Formation in angular unconformity on the eastern slope of the SCScp differs in the La Boca Canyon with respect to the north. In the south of the SCScp, a very coarse folded calcareous breccia appears (no obvious stratification is observed), made up of clasts up to 0.5 m, poorly classified, sub-angular and reworked fossils that transition into limy mudstone and wackestone strata with very thick layers; it has an undulating upper surface, turning black and darker gritty-looking appear. Towards the middle part of the formation, the lithologies that contain bituminous shale with nodules, alternate with bituminous limestone and again acquire very coarse thicknesses for the limestone, and medium to thick layers of bituminous shale. From this point, the presence of calcareous sandstone begins in thick strata, interbedded with calcareous shale, but of slightly lighter colors interdigitated with limestone with a wackestone texture. This alternation crowns the formation.

In the north of the SCScp, the calcareous breccia (Fig. 7A) has a greater extension, forming very evident projections on the eastern slope. These limestone clasts gradually become darker, with a wackestone texture, whose allelochemicals are slightly reworked fragments of ostracods, gastropods, foraminifera, echinoderms and bivalves, among others. Towards the upper part of the ledge, thick and very coarse strata (between 0.30 and 1.2 m) of mudstone-textured limestone with load-bearing structures at the top and at the base, with diagenetic stylolites, begin to be observed. The succession continues with alternating colors, sometimes darker or lighter until the formation is crowned. The most characteristic feature here is the absence of bituminous shale and calcareous sandstone. The lower contact is discordant due to the thrust of the SCScp, and the upper is transitional where the first flint bands appear in very coarse limestone strata.

4.2.2. San Ángel Formation

Longoria and Dávila (1979) in the La Boca canyon of the SCScp, measured 682 m of monotonous limestone succession with coarse to very coarse stratification, homogeneous gray to black with flint nodules, clayey limestone at the base and frequent diagenetic stylolites. Due to its faunal content, it is associated with a deep-water environment deposited from the Berriasian to the lower Aptian age. This formation is the deepwater equivalent of the Cupido Formation, and differs from the Tamaulipas Formation by the flint and clayey limestone at the base (Longoria, 1998).

In the study area, it has a minimum thickness of 986 m in the north, and a maximum thickness of 1262 m in the south; it is exposed in 24.44% of the study region, and its base appears at an elevation of 408 m a.s.l. on the eastern slope, and the top at an elevation of 1151 m a.s.l.on the western slope. The folding of this formation has a NW 20° - 60° SE strike with dips of 36° - 55° SW.

The appearance of medium to thick flint bands (from 8 to 15 cm), and the predominance of coarse and very coarse limestone strata with a mudstone or wackestone texture (Fig. 7B), marks the beginning of this formation, located on both the eastern and southern slopes, in the upper part of the western portion of the SCScp. Stratigraphically upwards, very coarse strata (from 1 to 2.5 m) of wackestone-textured limestone with ovoid morphology flint nodules and calcareous nodules with ammonites, and occasional ammonite impressions are observed. Towards the top, the very coarse wackestone-textured limestone, with calciespheres, radiolarians, and calpionellids, is lighter in color, with occasional small nodules of flint and iron oxides. In general, the succession presents load casts at the base of the diagenetic strata and stylolites. The upper contact is transitional, and it is defined to be below the first outcrops of thin calcareous shale interbedded between very coarse limestone strata.

4.2.3. La Peña Formation

This formation was described by Imlay (1936) in the sierra de Parras, Coahuila, as a succession of limestone and shale. The author informally divided it into a lower member of coarse limestone slightly interspersed with shale, and an upper member made up of alternating limestone and shale with thin bedding.

It has a minimum thickness of 80 m in the south and a maximum thickness of 138 m in the center-south portion of the study area; it is exposed in 2.53% of the research area, and it is exposed between elevations ranging from 418 to 952 m a.s.l. on the western slope of the mountain range. The fold of this formation has a NW 15° - 25° SE strike with dips 30° - 48° SW.

The base of this formation is recognized by the appearance of calcareous shale in medium to thick strata, which is interspersed with very coarse and thick strata of dark gray limestone. In the middle part of the unit, a dark gray calcareous foliated shale predominates (Fig. 7D), and limestone strata appear again at the top in transition towards the upper contact; it was defined in the last appearance of thin calcareous shale. This formation is characterized by being susceptible to intense erosion due to the terrigenous material content.

Fig. 7D shows a wackestone depositional texture, whose most abundant microfossils are planktonic foraminifera, echinoderm spicules, a few planktonic foraminifera, and calciespheres. As a mineralogical component, there is some content of iron oxide.

4.2.4. Tamaulipas Formation

Muir (1936) indicates that the term Tamaulipas limestone was used by Stephenson in 1921 in a private report for an oil company, and Belt makes the first mention of this formation in 1925. The author describes it in the Tamaulipas mountains as a gray micritic limestone with abundant layers of black flint in medium to thick strata, in a monotonous and homogeneous succession. The author subdivides it into three units: lower, Otates and upper; proposing the La Borrega canyon as the type locality. Longoria (1975) formally divides it into: La Borrega Limestone Member, Otates Limestone Member and Nacimiento Limestone Member; although he also indicates that this division is not perceptible in the Nuevo León region due to a change in facies. He assigns the age from Hauterivian to Aptian.

In the study area, the Tamaulipas Formation has a minimum thickness of 57 m in the north and a maximum thickness of 117 m in the south; it is exposed in 2.72% of the research area, and it is exposed between elevations ranging from 418 to 900 m a.s.l. on the western slope of the mountain range. The fold of this formation has a NW 12° - 60° SE strike with dips 20° - 62° SW.

This formation begins with very coarse strata consisting of light gray limestone, with diagenetic and tectonic stylolites, as well as load casts. Towards the middle part of the formation, some nodules of iron and flint appear, and then disappear towards the top, which is crowned by strata more than 2 m thick. The upper contact is transitional, and it is determined to be in the first thick layers of limestone with undulating or flat surfaces.

Fig. 7E shows a limestone with a mudstone texture with planktonic and benthic foraminifera, and calpionellids. Mineralogical components include fissures filled with calcite and few nodules of iron oxide.

4.2.5. Cuesta del Cura Formation

This formation was formally designated by Imlay (1936) in the sierra de Parras. It consists of a succession of dark gray to black undulating thin-medium deep-water limestone exposures, 64 m thick, interbedded with black chert. He assigned it an Albian age including the massive limestone up to 15 m thick that caps the formation.

In the study area it has a minimum thickness of 97 m in the south, and a maximum thickness of 139 m in the north; it is exposed in 3.65% of the research area, and it is exposed between elevations ranging from

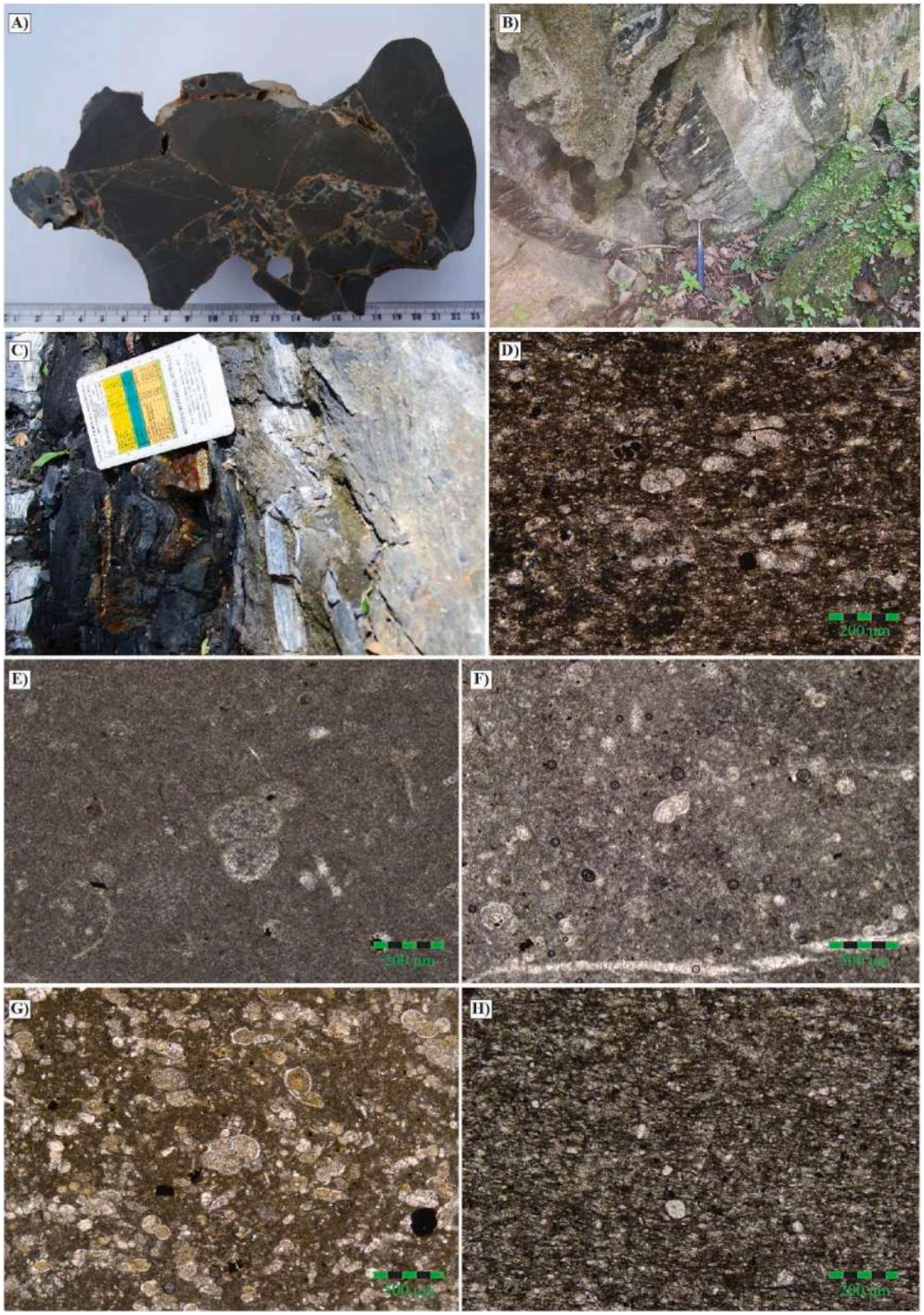

Fig. 7. A) Breccia of limestone intraclasts in very coarse strata in the north of the La Casita Formation (scale in centimeters); B) Flint bands up to 50 cm thick at the northern base of the San Ángel Formation (0.33 m geologist's hammer); C) Convoluted lamination in bituminous shale from the upper part of the Agua Nueva Formation, containing veinlets filled with calcite and pyrite (scale in centimeters and inches). Thin section photomicrographs: D) Foliated calcilutite from the middle portion of the La Peña Formation containing banded benthic foraminifera of organic matter and opaque minerals (LP-02h); E) Limestone from the Tamaulipas Formation with a mudstone texture with planktonic foraminifera and mollusk fragments (Ta-03h); F) Limestone from the upper part of the Cuesta del Cura Formation with a wackestone texture containing planktonic foraminifera, calcispheres and radiolaria (mNa-01A); G) Limestone from the middle part of the San Felipe Formation with a packstone texture, containing abundant planktonic foraminifera and occasional opaque minerals (SF-01); and H) Foliated calcilutite from the middle portion of the Méndez Formation with banded calcite crystals of organic matter and opaque minerals (mPr-01).

420 to 804 m a.s.l., on the western slope of the mountain range. The fold of this formation has a course NW 02° - 35° SE with dips 36° - 47° SW.

The lower part of the Cuesta del Cura Formation is characterized by an alternation of medium strata of limestone with radiolarians and dark gray to black argillaceous limestone, with thin layers of lamellar shale. In the middle part of the unit, the thickness of the limestone strata increases into a coarse limestone, characterized by a distinctive undulating stratification with chert interbedding in the form of bands, lenses or nodules and some diagenetic stylolites; occasionally, there is an alternation of clayey limestone in medium thicknesses. In the upper part, medium strata of limestone predominate, with bands and nodules of flint, alternated with strata of equal proportions of clayey limestone and bituminous shale. The upper contact is transitional, and it is defined when the last bands of flint disappear.

Fig. 7F identifies a limestone with a wackestone depositional texture, whose skeletal grains are made up of planktonic and benthic foraminifera, calpionellids, radiolaria and calcispheres. There is a high content of nodules and bands of iron oxide.

4.2.6. Agua Nueva Formation

The first formal use of the Agua Nueva Formation name is attributed to Muir (1934), who described it in the La Borrega canyon, in the Tamaulipas mountains. At its type locality, it is about 90 m, and consists of limestone with thin chert horizons interbedded with black carbonaceous shale and thin bentonite horizons.

In the study area it has a minimum thickness of 176 m in the north, and a maximum thickness of 218 m in the center-south; it outcrops in 4.74% of the research area, and it is exposed between elevations ranging from 450 to 748 m a.s.l., on the western slope of the mountain range. The fold of this formation has a course NW 05° - 26° SE with dips 21° - 50° SW.

The base of the Agua Nueva Formation is identified in the field by the appearance of thick strata with flat upper surfaces and bases of dark gray to black limestone in parallel lamination, alternating with medium strata of calcareous shale. Towards the middle part of this unit, the limestone is reduced in thickness, appearing with interbedded calcareous shale. The upper part is characterized by strata of oil shale with scattered pyrite crystals and calcite veins (Fig. 7C). In addition, in this part of the unit, a greater intercalation of limestone and clayey limestone is observed. Its upper contact is difficult to appreciate, because it is transitional and varies between outcrop exposures. For this reason it has been defined in the last strata of calcareous shale and bituminous shale that contain iron oxides or where coarse limestone already predominates with respect to the shale.

4.2.7. San Felipe Formation

The name San Felipe was initially used by G. Jeffreys in an internal report for the oil industry in 1910; however, Muir (1936) formally defined this formation as a Coniacian to Lower Santonian succession of limestone and shale. They define the type area to the west of the town of the same name on the railroad track that leads to Ciudad Valles-Tampico with a variable thickness ranging from 120 to 158 m.

In the study area it has a minimum thickness of 161 m in the north and a maximum thickness of 193 m in the south; it outcrops in 5.12% of the investigated area, and it is exposed between elevations ranging from 448 to 654 m a.s.l. on the western slope of the mountain range. The fold of this formation has a course NW 07° - 30° SE with dips 34° - 73° SW.

The rhythmic *flysch* type alternation of very coarse, thick and medium strata of limestone and calcareous shale characterizes this formation. The coloration of the formation is generally light brown with reddish tones in some portions. Occasional convolute stratification and wood fragments are observed, but the green volcanic ash that outcrops in this formation to the west and south was not observed in the area (Martínez-Paco et al., 2022; Velasco-Tapia et al., 2016). The upper contact is transitional, and it is defined when thick shale predominates over thick limestone.

Figure G shows a limestone with a packstone depositional texture; the content of skeletal grains is represented by abundant peloids and planktonic foraminifera.

4.2.8. Méndez Formation

Muir (1936) mentioned that the Méndez name was first used by Jeffreys in an unpublished report of an oil company in 1910; however, it was formally proposed by De Golyer in 1915. Both authors have defined the type locality, of the Maastrichtian, at 300 m east of the Méndez Station on the Tampico-Ciudad Valles railroad track, where very coarse strata of reddish shale outcrop, which due to meteoric effects, commonly present spheroidal exfoliation.

In this study, it outcrops on the eastern margin of the Huajuco Canyon with a minimum thickness of 767 m in the center-south, and a maximum thickness of 1044 m in the north; it is exposed between elevations ranging 440–614 m a.s.l. In this area it presents strikes of NW 18°-45° SE with dips of 18°-78° SW, and it is often covered erratically by soil and alluvial material. It is also exposed on the eastern slope of the mountain range due to tectonic contact, presenting elevations between 390 and 748 m a.s.l. The stratification in this area has a strike of NW 28° - 35° SE with inverted dips of 49° - 75° NE.

Very coarse layers of dark gray (light brown or yellow when exposed) foliated calcareous shale characterize the outcrops at the base and middle of the formation, which is strongly folded and fractured. Towards the upper part of the formation, a rhythmic succession of limestone and calcareous shale of highly variable thickness predominate. On the surface of the dark gray limestone, it is possible to observe sedimentary structures such as ripples, bioturbation, erosion marks and drag marks.

Fig. 7H indicates a limestone with wackestone depositional texture that contains skeletal grains represented by planktonic foraminifera. As mineralogical components, there are veinlets filled with calcite and iron oxides in less quantity.

4.3. Structural geology

In the SCScp, the folds, faults, and fractures behave as follows: the most relevant structural feature for understanding the geometry of the SCScp is given by a thrust fault called Las Moras (Romo-Ramírez et al., 2021) that affects this structure on its eastern flank, placing Upper Jurassic rocks in contact with Upper Cretaceous rocks, in a NW-SE orientation with vergence towards the NE. Such faulting is well evidenced by strongly recrystallized strata of limestone. Other structural elements that mark the deformational style of the SCScp are secondary reverse faults recorded in the San Ángel and Tamaulipas formations, with a NW-SE orientation and dips of 35° to the NE and with displacements of 0.30 m on average. In turn, the succession of these formations is controlled by shear fractures with a NW-SE orientation whose dips vary from 27° to 36° to the SW, in addition to NE-SW tensional fractures with dips of 85° to the NW and diagenetic tectonic stylolites. In this same sector, kinematic indicators such as fault striations, whose pitch is 20° to the W, were documented; they show the existence of a lateral fault with a NE-SW direction with dips that vary from 78° to 84° to the SW. In addition, recrystallized calcite fibers were identified, indicating a left lateral movement.

The folding style in the SCScp is linked to the contrast in the stratigraphic competition, encompassing the Agua Nueva, San Felipe and Méndez formations. The first two formations are characterized by mesofolds of asymmetric anticlines, with an axial plane to the NW-SE, a moderate inclination, and with a tight interlimb angle. These mesostructures are accompanied by shear fractures with a NE-SW orientation and dips, ranging from 70° to 81° to the NW and NW-SE with dips between 55° and 62° to the SW. To a lesser extent, there are extensional fractures with a NE-SW orientation, having dips from 74° to 86° to the NW and convoluted veins filled with calcite. The Méndez Formation is strongly folded, with abundant extensional and shear fracturing on the

western slope of the SCScp, accompanied by calcite-filled veining.

5. Geochemometrics

5.1. Spring water sampling

The groundwater sampling of each spring was performed during the dry season, where the mixture of runoff water with that arising from the springs is minimized. The records of the field readings are presented in Table 3. It also includes the average, maximum, minimum and standard deviation of each measured parameter.

The rainwater and the groundwater from the five springs that emerge in the SCScp during the dry season have a neutral pH ranging from 6.27 to 7.8 units, with dissolved oxygen between 26.5 and 97.2 percent, a positive ORP between 108.5 and 227.9 mV, and a temperature varying between 7.8 and 35.2 °C. The behavior of pH and ORP are characteristic of shallow groundwater as illustrated in Fig. 8.

The El Bañito thermal spring has unique characteristics that differentiate it from the rest of the springs in the study area, the most relevant feature is its high temperature, and also its readings which are almost twice the average for electrical conductivity, salinity and total dissolved solids. Fig. 9 shows how the springs found on the slopes of the mountain range (mMo, mNa and mLI) begin their enrichment in solutes, which continue to increase as the water descends between the rocks of the mountain range until it reaches the level of the shallow aquifer. Groundwater from the mPr has more dissolved solutes than the springs mentioned above, since it is found at the base of the mountainside, the water that infiltrates interacts with the shallow aquifer that feeds the perennial stream La Chueca.

5.2. Analytical results

Table 4 contains the complete results for each parameter analyzed for each sample from the five different springs. Fig. 10 shows the statistical graphical behavior of all trace elements, rare earths and major anions, which were above the detection limits of the representative analytical methods.

In all the analyzed samples, the Br, NO_2, PO_4, CO_3, and OH ions were below the detection limits of the analytical method. Eu was absent within the group of light rare earth elements and Lu, Tm, Ho and Tb, as part of the heavy rare earth elements, were also absent. The trace elements that were below the detection limits of the analytical method for all the spring water samples included are: Be, Al, Cr, Fe, Nb, Ag, Sn, Te, Hg, W, Pb and Bi.

A statistically-consistent and robust multidimensional classification from the 5 springs is presented in Fig. 11 (Verma et al., 2021).

The mMo and mNa found in the upper part of the mountain range are chemically simpler (Table 5), Ca–HCO_3 type. When interacting with the shallow aquifer on the western slope at the mPr, the water is Ca–Na–SO_4–HCO_3 type. On the eastern slope, the mLI is Ca–Na–HCO_3–SO_4 type, probably due to its interaction with calcareous shale rocks, bituminous shale, flint lenses and limestone. The groundwater of the mEB is the one with the highest enrichment in solute,s due to its journey to greater depths and its transit through evaporite rocks, and it is Na–Ca–SO_4–HCO_3 type.

The behavior of Sr (from the group of alkaline earth metals), Se (from the non-metal group), and Cl (group of major anions) clearly show the gradual chemical enrichment (Fig. 12) that occurs when rainwater infiltrates through the high elevations of the mountain range (mMo, mNa and mLI springs), to slowly reach the shallow aquifer through the sedimentary succession (mPr); each with solutes characteristic of the formations they pass through.

In the case of mEB, its enrichment is much greater, since the water goes through a long and deep path. This is evidenced by both its high comparative thermal gradient, and by containing a much higher concentration of Li and Cs (group of alkali metals), which are good indicators of long residence times and groundwater trajectories (Edmunds and Smedley, 2000), as they are absent in the mMo and mNa. The geochemical footprint of mEB, with the highest comparative concentrations of U, Tl, Ta, Ba, Mg, Rb, As, Ge, Zn, V and B, suggests that the geothermal reservoir must be found at depth.

The SI and the speciation minerals of the spring water (Table 6) shows evidence that its composition reflects, for the five springs, mineral species characteristic of a carbonate and evaporite succession, in which quartz is the only mineral that is saturated or close to saturation in all of them. Contrary to expectations, due to its high content of solutes, the groundwater of the mEB would be the most balanced, tending to corrosion.

5.3. Rare earth elements

The noticeable absence or low concentrations of light and heavy rare earths (Fig. 13) are recorded in the mMo, mNa and mLI; which is a natural behavior for “fresh” and alkaline groundwater (Noack et al., 2014). The emerging type mPr has the highest number and concentration of light and heavy rare earth elements. This is due to the fact that the groundwater of the regional aquifer circulates through Upper Cretaceous rocks of the San Felipe and Méndez formations, which includes volcanic ash between its calcareous strata (Martínez-Paco et al., 2022; Velasco-Tapia et al., 2016). Despite its high concentration of dissolved solids, conductivity and temperature, the mEB contains fewer elements, and a lower concentration of light and heavy rare earths; this is probably associated with the geochemistry that prevails in the evaporite rock reservoir where it forms, and its long trajectory during ascent to the surface, without ruling out that the bituminous shale strata of the La Casita Formation through which it passes could also capture mobile rare earth elements associated with the lithology (Ocampo-Díaz, 2011; Ocampo-Díaz et al., 2014). Further research is required to understand the geochemical behavior of rare earths in low-enthalpy geothermal systems emplaced in carbonate evaporitic sedimentary rocks.

Table 3
Measurements of field parameters of the springs.

ID	Date	Hour	Tu	Tam	Tag	Cond.	TDS	Sal	DO	pH	ORP
Rain	130221	13:00	6.80	13.9	7.8	102.6	0.0994	0.07	97.2	7.8	108.5
mMo	310121	13:10	0.25	23.4	19.4	395.6	0.2879	0.21	33.6	6.27	227.9
mNa	020221	13:35	2.77	22.0	17.6	406.9	0.3081	0.23	63.3	7.49	138.9
mPr	020221	12:01	0.28	22.1	21.7	852	0.5915	0.45	44.2	6.86	168.7
mEB	020221	11:15	0.35	22.3	35.2	1309	0.7085	0.53	36.7	6.89	182.6
mLI	020221	9:30	0.00	16.1	21.9	417.9	0.2886	0.21	26.5	7.00	151.5
Average			1.7	20.0	20.6	580.7	0.3807	0.28	50.3	7.05	163.0
Maximum			6.80	23.4	35.2	1309	0.7085	0.53	97.2	7.8	227.9
Minimum			0	13.9	7.8	102.6	0.0994	0.07	26.5	6.27	108.5
Standard Deviation			2.68	3.9	8.8	429.8	0.2251	0.17	26.2	0.53	40.8

Note: Tu: turbidity (NTU); Tam: ambient temperature (°C); Tag: water temperature (°C); Cond: electrical conductivity (μS/cm); TDS: total suspended solids (g/l); Sal: salinity (0/00); DO: dissolved oxygen (%); pH: hydrogen potential (0–14); ORP: oxidation-reduction potential (mV).

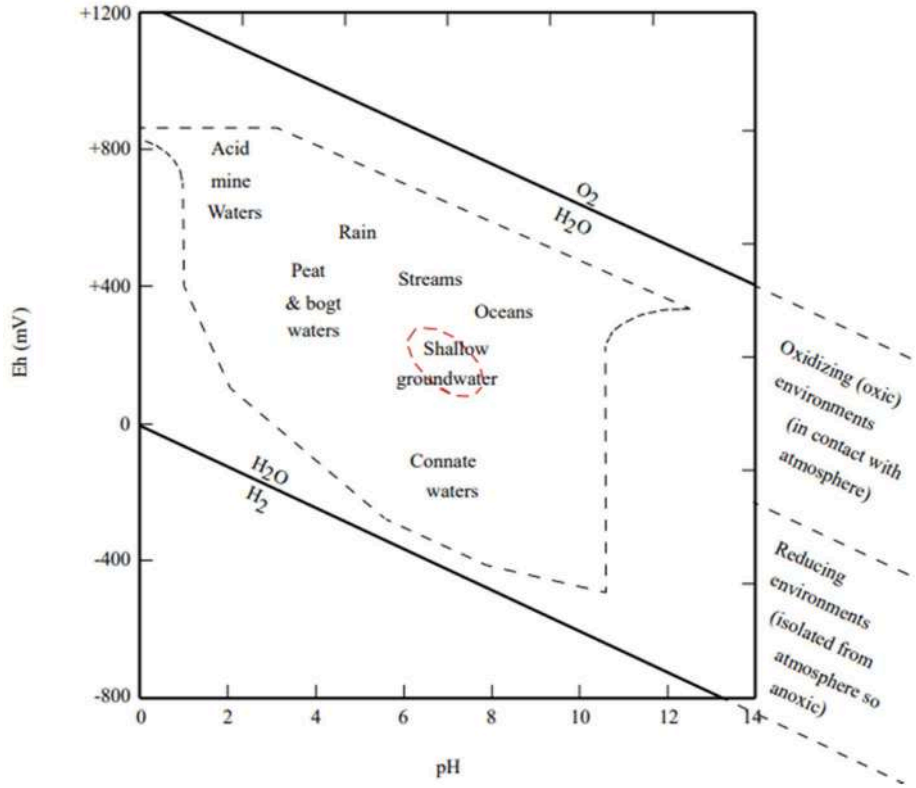

Fig. 8. Eh and pH dispersion graph of rainwater, runoff, seawater, groundwater and connate; the SCScp springs are illustrated within the red dotted lines (modified from Gill, 2015).

5.4. Water isotopes

The isotopic behavior of oxygen and hydrogen in the SCScp springs is illustrated as Fig. 14. Equation (1) describes the linear correlation for both variables in the SCScp groundwater, with a correlation coefficient $R^2 = 0.99$.

$$\delta D = 8.2\delta^{18}O + 16.42 \quad (1)$$

Where δD is the isotopic composition of deuterium, and ^{18}O is the heavy oxygen isotope, with respect to Vienna Standard Mean Ocean Water (VSMOW), both in parts per thousand. This representation was compared with respect to the meteoric water flow line (LAMSMO), the runoff capture water line (LAESMO) of the Sierra Madre Oriental (Aguilar-Ramírez et al., 2017), and the Mexican groundwater line (LASM) (Wassenaar et al., 2009), equations (2)–(4) respectively. It is evident that the springs of the SCScp have a meteoric water origin in an arid climate, with rapid infiltration clearly influenced by altitude and temperature. The ranges of variation for both the oxygen isotopes and deuterium are wide, as in the mMo spring that originates in the upper part of the mountain range, whose groundwater has a very short residence time; in contrast to the mEB, whose groundwater has a long residence time and transits at greater depths between the geological formations of a deep sedimentary basin.

$$\delta D = 8.15\delta^{18}O + 15;\ R^2 = 0.99 \quad (2)$$

$$\delta D = 8.32\delta^{18}O + 16;\ R^2 = 0.99 \quad (3)$$

$$\delta D = 7.9\delta^{18}O + 6.4;\ R^2 = 0.95 \quad (4)$$

The two springs that originate in the upper part of the mountain range, and that flow mainly through Cretaceous carbonate rocks, mMo and mNa, had isotopic ratios of $^{87}Sr/^{86}Sr$ of 0.70757 and 0.7076, respectively; which fall within the upper range of 0.7072–0.7076 published by Lehmann et al. (1999) and by Wolaver et al. (2013) for sedimentary rocks from the Sierra Madre Oriental of Barremian to Albian age.

The mPr groundwater, with an $^{87}Sr/^{86}Sr$ ratio of 0.70744, closely resembles the ratios of the Cuatro Ciénegas springs reported by Wolaver et al. (2013). This author concludes that the contribution of Sr in the water of the springs comes mainly from the Cretaceous carbonates that underlie such region.

The groundwater of the mLI has an $^{87}Sr/^{86}Sr$ ratio of 0.70804, and the groundwater of the mEB of 0.70847, which is very high for the data reported in the Upper Jurassic-Upper Cretaceous sedimentary succession.

5.5. Low enthalpy geothermal system "El Bañito" (SGBEEB)

The thermal water that emerges in the mEB forms in a folded sedimentary basin that possibly includes Callovian or earlier evaporitic rocks at depth (Goldhammer and Johnson, 2001). Geothermometric calculations in this type of geological systems with moderate flows and low enthalpy are complex, and have not been thoroughly studied in the world (Blasco et al., 2017, 2018; Billarent-Cedillo et al., 2021). The classical geothermometers commonly used (Verma et al., 2008) were developed mainly in high-temperature geothermal systems associated with *pull apart* basins and volcanic arcs, so their usefulness in the SGBEEB should be complemented and used with caution. Using the Na, K, Mg ternary diagram of Giggenbach (1988); the mEB groundwater is considered immature; that is, the water that rises from the reservoir mixes gradually or abruptly with the regional aquifer. In this study, the depth and temperature of the SGBEEB reservoir are inferred by three methodologies that complement each other and allow us to propose a first reasonable hypothesis, these are:

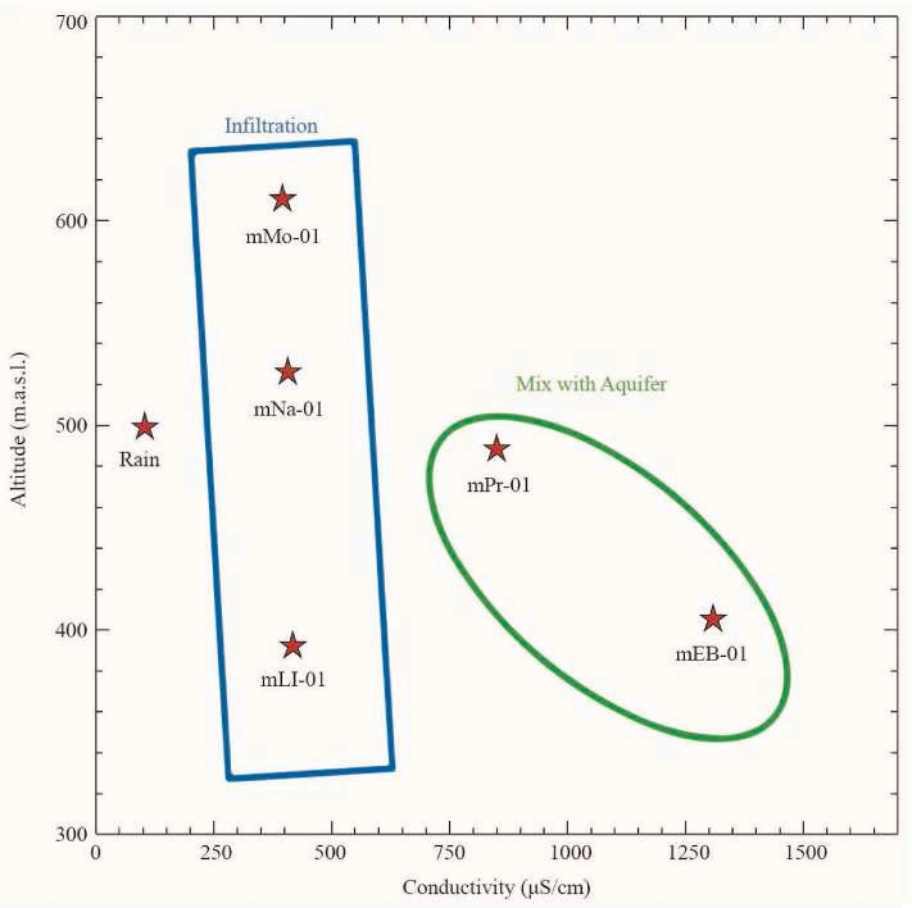

Fig. 9. Dispersion graph of the altitude and electrical conductivity of the spring groundwater.

5.5.1. Depth inference of evaporitic rocks and their thermal gradient

The conjugation of the Pacific and Atlantic tectonic-sedimentary processes caused continuous exhumation of basement uplift including the Tamaulipas Arch (Ocampo-Díaz et al., 2022). Goldhammer and Johnson (2001, Fig. 11) propose that a sedimentation of evaporite rocks in a *sabkha* environment ocurred during the Callovian and early Oxfordian in the Monterrey Trough; however, these rocks do not outcrop in the SCScp. Eguiluz de Antuñano (1991, Fig. 8) locates the "structural high called Isla de San Carlos" very close to the east of the SCScp, by the interpretation of data from the Margaritas-1, Ramones-1, Carruaje- 1, Suarez-1, Terán-1 and El Benemerito-1 oil wells, and seismic sections (low resolution 2D). This implies that the SCScp is found in the portion of the sedimentary wedge caused by the Tamaulipas Arch. Eguiluz de Antuñano (2001, Fig. 4, Table 1) shares information from the Ramones-1 oil well, where a powerful collection of halite, gypsum and dolomite are in an interval between 1579 and 2075 m deep; but the Terán 1 well has no longer evaporites, and cuts granodioritic rock at a depth of 1402 m. By extrapolating the evaporite thicknesses from the structural high to the east, it could be determined that the geothermal reservoir would then be over 1500 m deep. The geostatic pressure can be calculated with Equation (5), which describes the pressure regime in a stratigraphic unit that exhibits higher lithostratographic pressure than the hydrostatic pressure in its pore structure (Khan and Islam, 2007).

$$P_g(z) = P_0 + g\int_0^z \rho(z)dz \tag{5}$$

Where $P_g(z)$ is the geostatic pressure at depth z in Pa; ρ is the density of the overlying rocks at depth z in kg/m^3; g is the acceleration due to gravity in m/s^2, z is the depth in m; and P_0 is the surface pressure in Pa, resulting in $P_g(z) = 38$ MPa; for a $\rho = 2600$ kg/m^3 (average value of limestone and shale rocks); $g = 9.778$ m/s^2; $z = 1500$ m and $P_0 = 92{,}990$ Pa, which was obtained from the average of historical data from the Cumbres de Monterrey El Diente automatic weather station (SMN, 2021).

The "anomalous" increase in the thermal gradient at depth, can then be justified by the greater presence of salt in the evaporite rocks, as it has been shown that the thermal conductivity increases two to four times more, compared to other carbonate sediments. The heat is channeled through the salt, forming positive temperature anomalies towards the top, and lower temperatures towards the base (Daniilidis and Herber, 2017).

In this way the El Bañito geothermal reservoir potentially arises in the upper part of the evaporite rocks (which do not outcrop in the mountain range) at a depth of less than 1500 m, with a geostatic pressure of less than 38 MPa, and a temperature of less than 100 °C.

5.5.2. Geothermometric modeling

The geothermometric modeling provides a more generalized approach than the classical chemical geothermometry, because this process simulates, for a group of selected minerals (due to their possible presence in the geothermal reservoir), a progressive increase in temperature to obtain a range in the SI in which they simultaneously reach equilibrium (Blasco et al., 2019). When two or more of the selected minerals indicate a similar range of temperature equilibrium, the average temperature can be considered the best estimate.

Temperature ranges from 35 °C (mEB upwelling temperature) to 100 °C were modeled for the group of selected minerals: quartz, dolomite, calcite and anhydrite. Fig. 15 shows the equilibrium interval of quartz and dolomite that cross very close to SI = 0 at 67 °C; similarly,

Table 4
Analytical results of the water from the springs.

Analyzed parameter	mMo	mNa	mLI	mPr	mEB	Average	Standard deviation
Major Cations (μg/l)							
Na^+	*1490*	2160	4860	9800	**75900**	18842	32063
K^+	320	*80*	770	930	**3280**	1076	1278
Li^+	<1	<1	5	5	**56**	22	29
Ca^{2+}	*85300*	91200	86100	**193000**	142000	119520	47420
Mg^{2+}	3640	4230	*2140*	5630	**8730**	4874	2493
Major Anions (mg/l)							
F^-	0.06	*0.05*	0.07	0.07	**0.13**	0.076	0.031
Cl^-	*2.8*	3.01	5.84	9.11	**102**	24.552	43.370
Br-	<0.1	<0.1	<0.1	<0.1	<0.3	NA	NA
NO_2^-	<0.04	<0.04	<0.04	<0.05	<0.1	NA	NA
NO_3^-	**1.67**	0.9	1.3	1.59	*0.54*	1.2	0.477
PO_4^-	<0.08	<0.08	<0.08	<0.01	<0.02	NA	NA
SO_4^-	*9.88*	13	35.3	**213**	212	96.636	106.223
CO_3^{2-}	<1	<1	<1	<1	<1	NA	NA
OH^-	<1	<1	<1	<1	<1	NA	NA
HCO_3^-	235	253	208	**293**	*190*	235.8	40.121
SiO_2	6	6	9	**20**	18	11.8	6.723
Isotopes							
$\delta^{18}O$ ‰	**−7.11**	−6.76	−5.87	−6.68	*−5.56*	−6.396	0.652
δ D ‰	**−41.8**	−39.0	−31.4	−38.7	*−29.4*	−36.06	5.353
$^{87}Sr/^{86}Sr$	0.70757	0.70760	0.70804	*0.70744*	**0.70847**	0.70782	0.00043
Light Rare Earths (μg/l)							
La	*0.002*	0.005	0.004	**0.009**	0.005	0.005	0.003
Ce	<0.001	0.001	<0.001	<0.001	<0.001	NA	NA
Pr	<0.001	0.001	<0.001	0.002	<0.001	NA	NA
Nd	0.003	0.005	0.003	**0.010**	0.003	0.005	0.003
Sm	<0.001	0.001	<0.001	0.002	<0.001	NA	NA
Eu	<0.001	<0.001	<0.001	<0.001	<0.001	NA	NA
Gd	0.019	0.020	0.021	**0.029**	<0.001	0.022	0.005
Heavy Rare Earths (μg/l)							
Sc	<1	<1	<1	<1	<1	NA	NA
Y	*0.010*	0.018	0.011	**0.048**	0.012	0.019	0.016
Lu	<0.001	<0.001	<0.001	<0.001	<0.001	NA	NA
Yb	<0.001	<0.001	<0.001	0.002	<0.001	NA	NA
Tm	<0.001	<0.001	<0.001	<0.001	<0.001	NA	NA
Er	<0.001	<0.001	<0.001	0.002	<0.001	NA	NA
Ho	<0.001	<0.001	<0.001	<0.001	<0.001	NA	NA
Dy	<0.001	0.001	<0.001	0.004	<0.001	NA	NA
Tb	<0.001	<0.001	<0.001	<0.001	<0.001	NA	NA
Trace Elements (μg/l)							
B	12	*9*	12	15	**66**	22.8	24.24
Be	<0.1	<0.1	<0.1	<0.1	<0.1	NA	NA
Al	<2	<2	<2	<2	<2	NA	NA
Si	*3000*	3100	4600	**10000**	9300	6000	3400.73
Ti	**0.8**	<0.1	0.3	0.2	<0.1	0.43	0.3
V	0.3	0.3	0.3	0.3	**0.5**	0.34	0.08
Cr	<0.5	<0.5	<0.5	<0.5	<0.5	NA	NA
Mn	0.3	0.4	0.4	0.4	<0.1	0.37	0.05
Fe	<10	<10	<10	<10	<10	NA	NA
Co	**0.031**	0.028	0.021	0.026	<0.005	0.021	0.004
Ni	<0.3	0.3	**0.6**	0.4	0.4	0.425	0.12
Cu	**0.4**	0.3	<0.2	<0.2	<0.2	NA	NA
Zn	<0.5	<0.5	1.2	<0.5	**15.5**	8.350	10.112
Ga	0.02	0.02	0.02	**0.03**	*0.01*	0.020	0.1
Ge	<0.01	<0.01	0.03	0.01	**0.16**	0.067	0.081
As	0.22	0.17	0.35	*0.16*	**0.84**	0.348	0.285
Se	*0.4*	0.5	1	1.1	**1.7**	0.940	0.522
Rb	0.064	*0.029*	1.28	0.164	**13.1**	2.927	5.710
Sr	*211*	229	240	733	**1090**	500.600	395.901
Zr	0.03	0.03	0.02	0.01	0.02	0.022	0.008
Nb	<0.005	<0.005	<0.005	<0.005	<0.005	NA	NA
Mo	*0.1*	0.2	1.9	1.4	**6**	1.920	2.408
Ag	<0.2	<0.2	<0.2	<0.2	<0.2	NA	NA
Cd	0.01	<0.01	0.01	0.01	<0.01	0.010	0.000
In	<0.001	<0.001	<0.001	<0.001	<0.001	NA	NA
Sn	<0.1	<0.1	<0.1	<0.1	<0.1	NA	NA
Sb	**0.13**	0.08	0.07	*0.04*	0.05	0.074	0.035
Te	<0.1	<0.1	<0.1	<0.1	<0.1	NA	NA
Cs	<0.001	<0.001	0.783	0.002	**8.12**	2.968	4.479
Ba	16.3	*13.4*	31.9	46.6	**49**	31.440	16.531
Hf	0.006	**0.008**	0.005	0.005	*0.004*	0.006	0.002
Hg	<0.2	<0.2	<0.2	<0.2	<0.2	NA	NA
Ta	0.003	0.004	0.003	0.004	**0.005**	0.004	0.001

(*continued on next page*)

Table 4 (*continued*)

Analyzed parameter	mMo	mNa	mLI	mPr	mEB	Average	Standard deviation
W	<0.02	<0.02	<0.02	<0.02	<0.02	NA	NA
Tl	0.003	*0.001*	0.015	0.002	**0.145**	0.033	0.063
Pb	<0.01	<0.01	<0.01	<0.01	<0.01	NA	NA
Bi	<0.3	<0.3	<0.3	<0.3	<0.3	NA	NA
Th	*0.168*	0.256	0.058	**0.326**	0.017	0.165	0.130
U	*0.205*	0.419	1.5	1.1	**1.82**	1.009	0.689

Note: NA: not applicable.

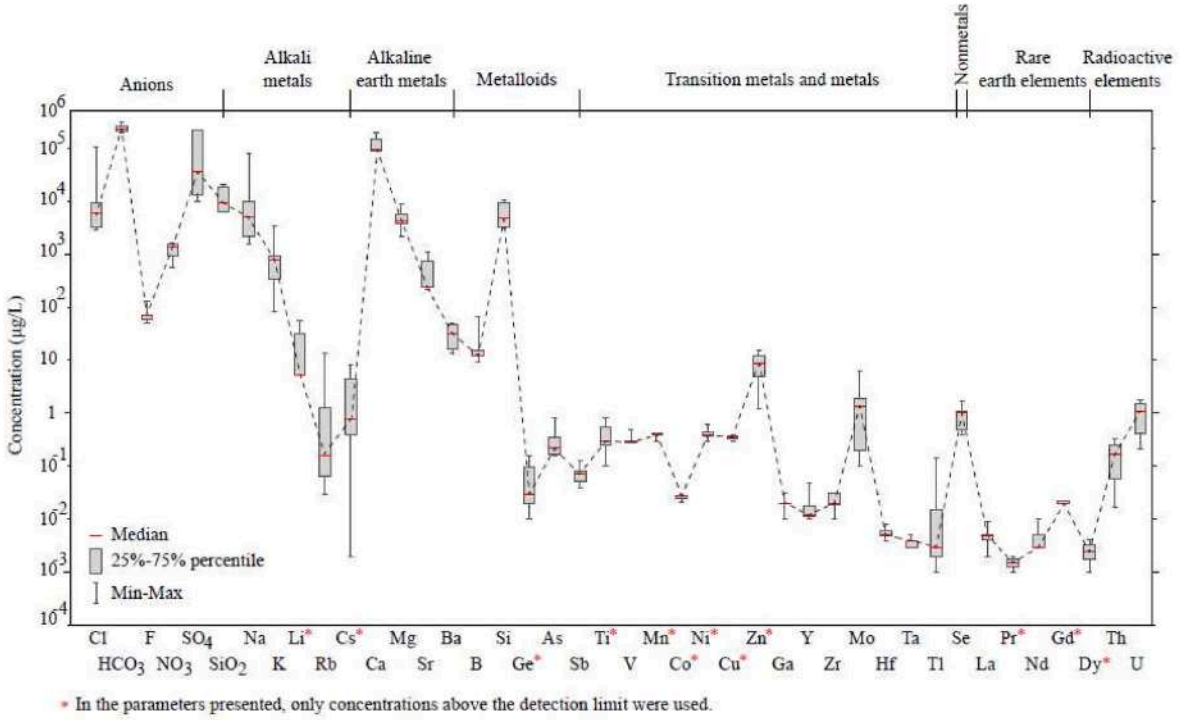

Fig. 10. Semilogarithmic statistical graph of the elements dissolved in the springs groundwater.

calcite intersects quartz very close to SI = 0 at 49 °C, and anhydrite does not converge according to the observed pattern. The phase shift of calcite and anhydrite at the SI = 0 junction with respect to quartz and dolomite may be due to CO_2 degassing processes during the ascent of the thermal water, and also to a greater imbalance when mixed with the aquifer water. Calcite precipitation is usually caused by loss of CO_2 from the hydrothermal system when hot solutions get close enough to the surface (Ellis, 1959), reaching equilibrium earlier and, therefore, in a lower temperature range than other minerals such as the ones shown in Fig. 15. Quartz was the least susceptible mineral to the changes of the aforementioned processes, its balance was considered the most stable, having a medium value between calcite and dolomite. With the geothermometric modeling, a temperature of the SGBEEB reservoir is established between 49 °C and 67 °C; the depth of the reservoir in this temperature interval ranges from 800 m to 1700 m.

The behavior of pore pressure in many sedimentary basins at depths less than 2000 m is similar to the hydrostatic pressure (Onajite, 2017). For the estimation of the pore pressure in the reservoir, Equation (6) was considered corresponding to a normal pore pressure, which is the hydrostatic pressure caused by the fluid column in the pore structure from the surface to the depth of concern (Zhang, 2013).

$$P_h = \rho_f g h \tag{6}$$

where P_h is the hydrostatic pressure in Pa, ρ_f is the density of the fluid in kg/m^3, g is the acceleration due to gravity in m/s^2, and h is the vertical height of the fluid column. The g was considered to be 9778 m/s^2; ρ_f is a function of salinity, temperature and dissolved gas content, so the value resulting from the PHREEQC modeling of the solution interval, at the lowest modeled reservoir temperature (49 °C) of 989 kg/m^3, and at the highest temperature (67 °C) of 979 kg/m^3; h is the depth of the modeled temperature interval of the reservoir from 800 m to 1700 m; therefore, the P_h was estimated to be greater than 7 MPa and less than 16 MPa.

5.5.3. Chemical geothermometers

Chiodini et al. (1995) proposed new geoindicators for aqueous solutions, from medium and low temperature hydrothermal systems (50–150 °C) that have been housed in carbonate-evaporitic rocks. Blasco et al. (2017) proposed the use of several geothermometric methodologies to screen and select those that match the expected real conditions. SiO_2-type geothermometers were selected to learn the characteristics of the SGBEEB (Table 7), which indicate a temperature range of the geothermal reservoir of 60 °C ±4, because the rest of the calculated geothermometers proposed temperatures below or close to the upwelling temperature of the El Bañito spring or above 70 °C.

5.6. Conceptual model

The anticline that forms the Cerro de La Silla Mountain range originates from the transpressive efforts of the Mexican Orogeny (Cenomanian-Eocene), and burial-exhumation processes that have exposed a

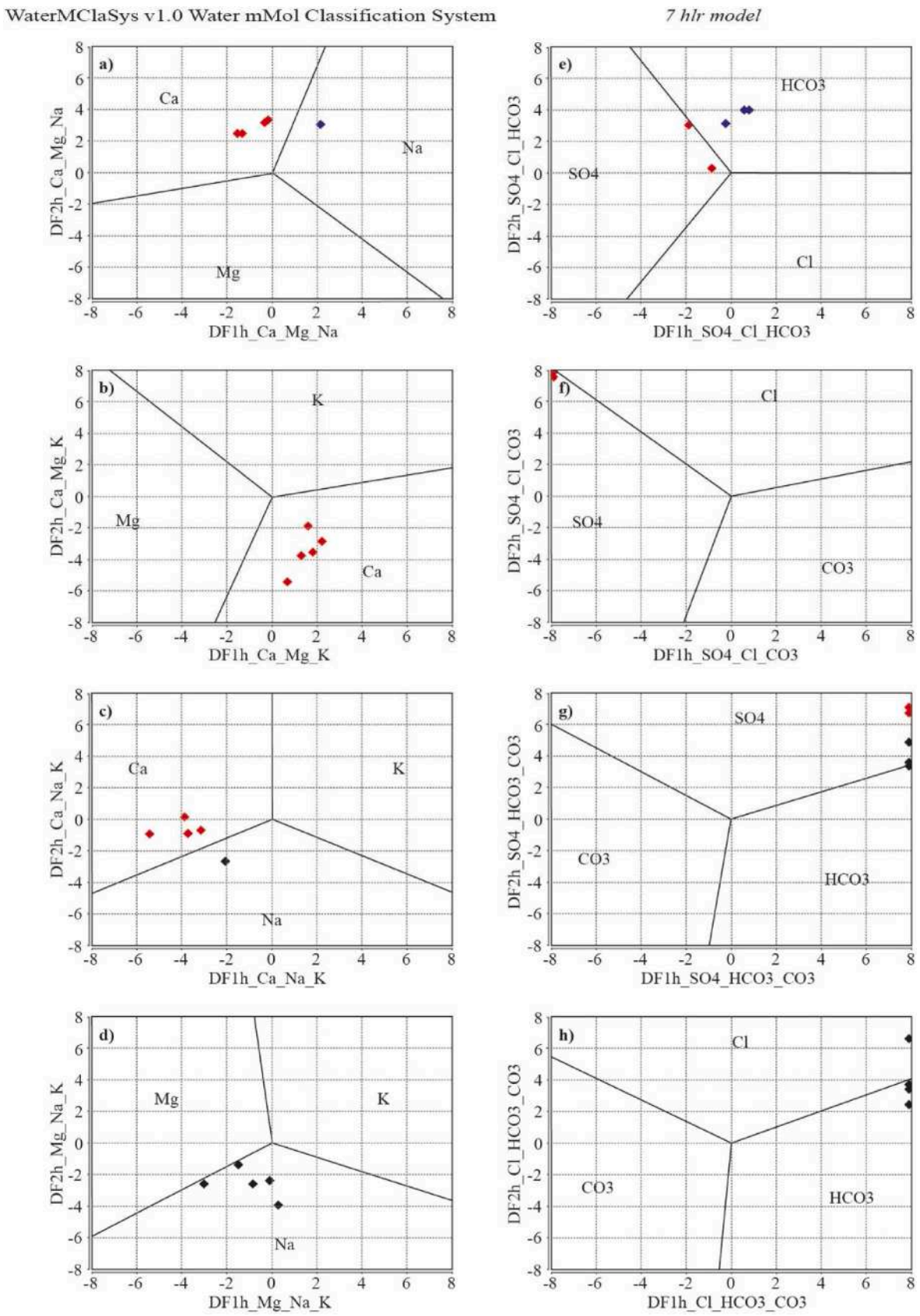

Fig. 11. Diagrams of the discriminant functions (DF1h-DF2h) for the log-hybrid relationships of the classes of cations (from a to d) and anions (from e to h) of the SCScp springs.

Table 5
Ionic classification of SCScp spring water.

I.D.	Classification. Model 7hlr	Confidence	Ion Imbalance (%)
mMo	Ca–HCO_3	Acceptable	5.625
mNa	Ca–HCO_3	Acceptable	5.192
mLI	Ca–Na–HCO_3–SO_4	Acceptable	4.384
mPr	Ca–Na–SO_4–HCO_3	Acceptable	5.243
mEB	Na–Ca–SO_4–HCO_3	Acceptable	3.500

Note. The percentage of ionic imbalance of spring water is within acceptable international limits of 5%.

powerful marine sedimentary succession from the Late Jurassic, Cretaceous, and Paleogene ages 30 million years ago. The folds, faults and fractures have evolved in an incipient karst that allows the infiltration of meteoric water, that as it flows through the rock strata is enriched in solutes and isotopes characteristic of these rocks. The pathway of the meteoric water in the interior of the mountain range forms perched water-bearing zones in the high and intermediate sections, to subsequently reach a groundwater base level where the regional aquifer is located; a peculiarity created by the association of an important thrust, an extensive right lateral fault, and a carbonate evaporite succession at depth that allowed the formation of what we have called the SGBEEB in this study.

With greater demand for groundwater from fresh water aquifers, there is potential for the generation of deep thermal water intrusion into the shallow regimes, as shown with extrapolated potable extraction well, resulting in a potential degradation of the groundwater quality (Fig. 16).

6. Discussion

The Cerro de La Silla Mountain range is a powerful succession of carbonated marine sedimentary rocks that constitute an important catchment area, as well as a rapid infiltration area with vertical displacement of meteoric water that recharges some aquifers of the MMA in the State of Nuevo León, México. The folds and thrusts formed during the Mexican Orogeny, the subsequent uplift of the crust, an incipient karst in carbonate rocks with abundant flint lenses/nodules, and a high content of organic matter, have contributed to generating an active surface hydrological network on the slopes of the SCScp; although it takes advantage of the ducts and cavities that have been formed, still restricts and obstructs the circulation and infiltration of meteoric water that descends from the upper parts of the mountain range, until it reaches its base flow in the regional aquifer. This is significantly different from the faster flow and infiltration regime that occurs in the south of the SMO in the El Abra mountain range, where most of the water infiltrates the upper parts of the tropical karst, and emerges very quickly in very large volumes through long and wide ducts and caves at the base level (Fish, 1977; Espinasa-Pereña and Nieto-Torres, 2015).

Due to its complex geology and its economic importance (groundwater, oil, gas and mining), Northeastern Mexico has been deeply studied by several researchers throughout time (Eguiluz de Antuñano, 1991, 2001; Goldhammer, 1999; Goldhammer and Johnson, 2001; González-Sánchez et al., 2007; Gray et al., 2001; Imlay, 1936; Ocampo-Díaz et al., 2016, 2022; Pindell et al., 2020). As a result of the different types and objectives of geological investigations performed in the region, the use of formal stratigraphic nomenclature/units became difficult too (Gamper, 1977; Lehmann et al., 1999; Longoria, 1984; Michalzik and Schumann, 1994). We discarded the use of the Zuloaga, Carbonera and Cupido formations, as proposed by Romo-Ramírez et al. (2021), because the descriptions of those units are different to the lithostratigraphic units identified in the SCScp.

The meteoric water that infiltrates the upper parts of the mountain range, which crosses the San Angel, La Peña, Tamaulipas, and Cuesta del Cura formations emerges in the mMo and the mNa as Ca–HCO_3 type groundwater, similar to the aquifer recharge water at the foot of the mountain range, and the water that flows through limestone and shale (Mora et al., 2017; CONAGUA, 2020). Relatively short circulation

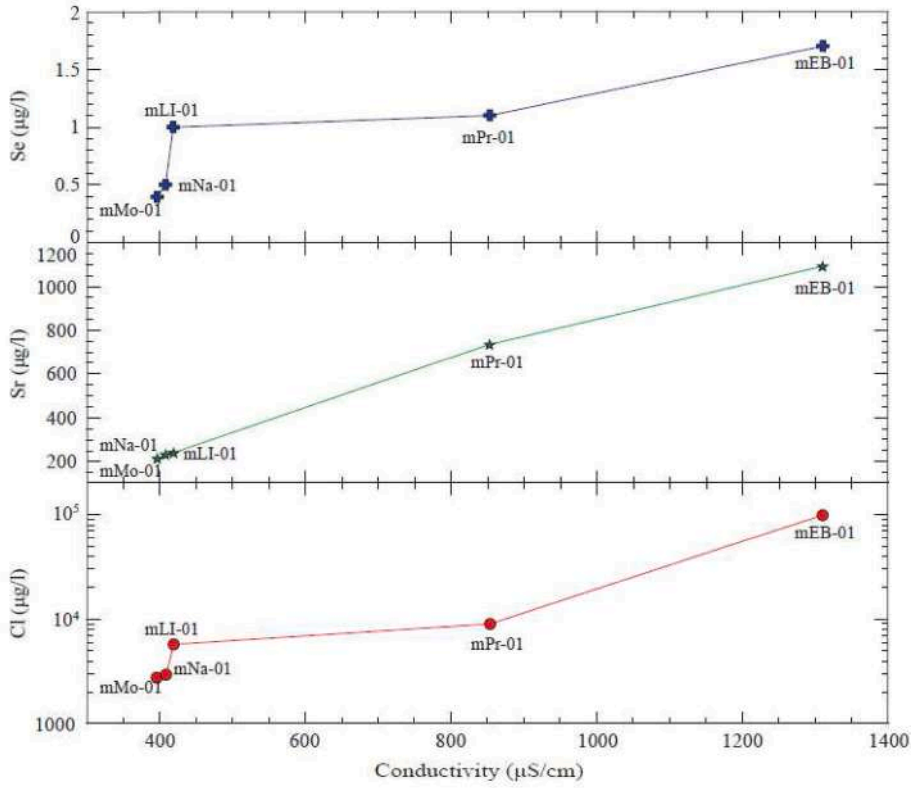

Fig. 12. Dispersion graph of Sr, Se and conductivity and semilogarithmic behavior of Cl, and conductivity in the groundwater of the SCScp springs.

Table 6
SI and speciation of the water of the SCScp springs.

	mPr	mNa	mMo	mEB	mLI
Anhydrite	−1.32	−2.71	−2.83	−1.30	−2.25
Aragonite	−0.15	0.14	−1.10	−0.25	−0.39
Barita	0.09	−1.36	−1.40	−0.01	−0.61
Calcite	−0.01	0.28	−0.96	−0.09	−0.25
$Cd(OH)_2$	−10.30	–	−11.35	–	−9.90
$CdSiO_3$	−9.33	–	−10.99	–	−9.27
$CdSO_4$	−13.37	–	−14.56	–	−13.93
Celestite	−1.68	−3.23	−3.36	−1.44	−2.75
Calcedonite	0.11	−0.36	−0.38	−0.09	−0.24
Crisotile	−10.13	−7.98	−15.24	−7.90	−10.92
$CO_2(g)$	−1.45	−2.15	−0.94	−1.58	−1.71
Dolomite	−1.23	−0.45	−2.96	−1.04	−1.77
Fluorite	−2.93	−3.36	−3.25	−2.68	−3.15
Gypsum	−0.97	−2.32	−2.46	−1.10	−1.91
$H_2(g)$	−26.36	−26.76	−27.31	−26.35	−26.05
$H_2O(g)$	−1.59	−1.70	−1.65	−1.25	−1.58
Halite	−8.64	−9.74	−9.93	−6.7	−9.10
Hausmannite	−19.86	−16.65	−23.07	–	−19.01
Magnetite	−6.96	−5.47	−7.67	–	−6.74
$O_2(g)$	−1.07	−0.91	−1.19	−1.16	−1.29
Octavite	−4.16	–	−4.71	–	−4.03
Pyrochroite	−9.98	−8.69	−11.17	–	−9.60
Pyrolusite	−10.37	−9.36	−10.99	–	−10.28
Quartz	0.55	0.09	0.06	0.31	0.20
Rodocrosite	−3.26	−2.70	−3.97	–	−3.15
Sepiolite	−6.65	−5.85	−10.80	−5.99	−7.77
Sepiolite(d)	−9.46	−8.55	−13.55	−9.15	−10.59
$SiO_2(a)$	−0.74	−1.23	−1.24	−0.89	−1.09
Smithsonite	–	–	–	−2.86	−3.98
Strontianite	−1.96	−1.82	−3.08	−1.83	−2.34
Sylvita	−9.21	−10.70	−10.14	−7.68	−9.45
Talc	−6.24	−5.10	−12.38	−4.24	−7.73
Willemite	–	–	–	−4.55	−7.56
Witherite	−4.13	−3.94	−5.08	−4.17	−4.13
$Zn(OH)_2(e)$	–	–	–	−4.75	−5.57

springs have been associated with this type of groundwater, in carbonate rocks (Montanari et al., 2017). The Ca–Na–HCO_3–SO_4 type groundwater of the mPr that crosses the San Felipe and the Méndez formations and reaches the base level, has mixed with the water of the Huajuco canyon regional aquifer, and it is relatively similar to the transitional water that flows in the Monterrey region (Mora et al., 2017). The mLI water, characterized as Ca–Na–SO_4–HCO_3 type, flows through the lower part of the San Angel Formation and the La Casita Formation with a certain similarity to the groundwater of the north and northeast of the MMA. The mEB water charecterized as Na–Ca–SO_4–HCO_3 type is the only known hot spring of the SGBEEB; this system (that does not outcrop in the Cerro de La Silla Mountain range), emerges through the La Casita Formation, but crosses deeper formations. In the SCScp springs, NO_3 was found in the range from 0.54 mg/L to 1.67 mg/L. The average of NO_3 (1.2 mg/L) is similar to 1 mg/L; nevertheless, the mBE presented the lowest concentrations (0.54 mg/L), lower than the average (almost half); this could indicate that the deep hot water ascends along the fractures and mixes with the shallow groundwater with low temperature, low TDS, and relatively high HCO_3 and NO_3 concentrations (Yang et al., 2019).

The noticeable absence and low concentrations of light and heavy rare earths are recorded in the mMo, mNa and mLI springs, which correspond to freshly-infiltrated water. The mPr spring has the highest number and concentration of light and heavy rare earth elements, due to the interaction of this spring with the Huajuco canyon aquifer, that circulates through rocks containing terrigenous material. The mEB spring contains fewer elements, and in lower concentration of light and heavy rare earths. There is no further information regarding this condition, so further research is required to better understand the geochemical behavior of rare earths in low enthalpy geothermal systems emplaced in carbonate-evaporitic sedimentary rocks.

The isotopes δD and $\delta^{18}O$ in the perennial springs of the SCScp, confirm the meteoric origin of the emerging waters; they are representative of the perched aquifers (mMo, mNa, mLI) of the upper part of the mountain range, of the regional shallow aquifer in the Huajuco Canyon (mPr); and they are also representative of the groundwater that circulates at greater depth (mEB) below the mountain range. These isotopes reflect a warmer-dryer paleoclimate in the northern part of the SMO, when compared to the LAMSMO and the LAESMO (Aguilar-Ramírez et al., 2017). They contrast even more when compared with the LASM (Wassenaar et al., 2009). This behavior is different from what occurs for geothermal and volcanic fields in converging tectonic plates of the Pacific (Giggenbach, 1992).

Low enthalpy systems in carbonate evaporitic systems have been comparatively understudied in México (Billarent-Cedillo et al., 2021), and less frequently studied in the world than those formed in tectonically active margins (Blasco et al., 2019). No geological and geochemometric information was found for other hot springs or low enthalpy geothermal systems emerging in the La Casita Formation. Pindell et al. (2020) report $^{87}Sr/^{86}Sr$ ratios of up to 0.709811 in halite

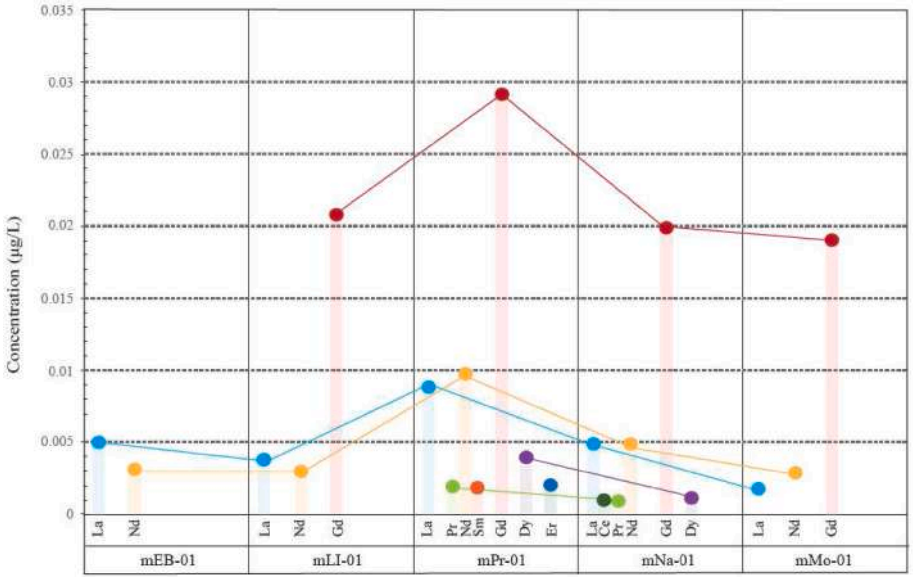

Fig. 13. Bar graph of the behavior of rare earths in the springs groundwater.

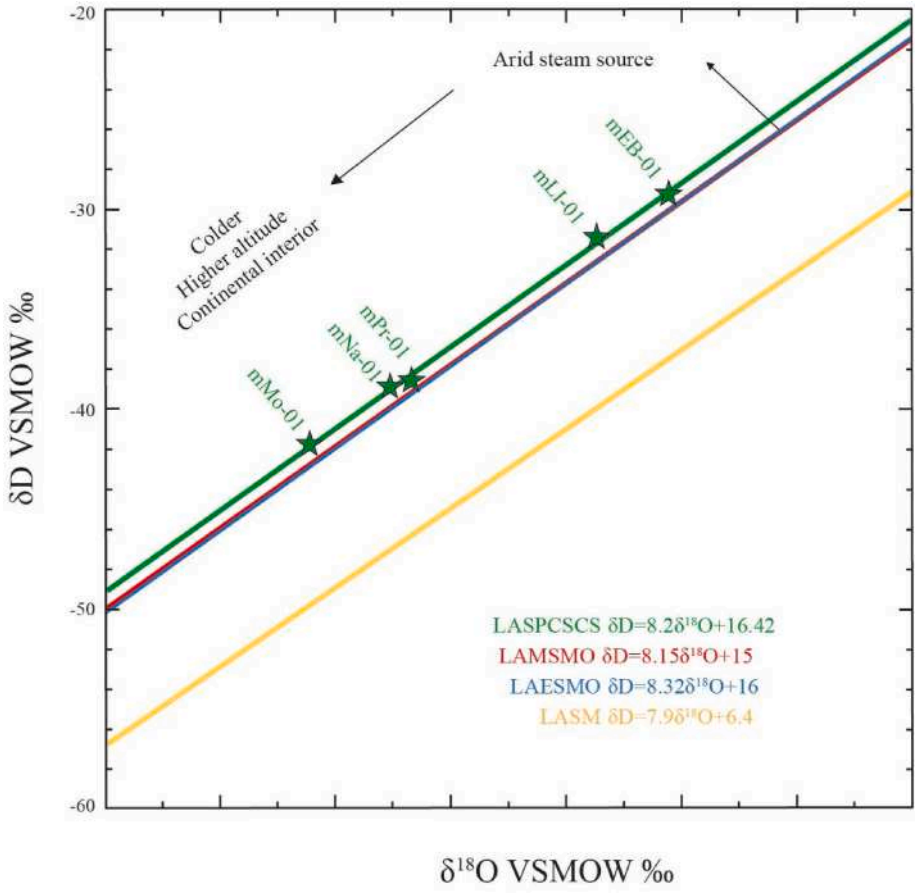

Fig. 14. Dispersion graph of δD and $\delta^{18}O$ of groundwater from SCScp springs.

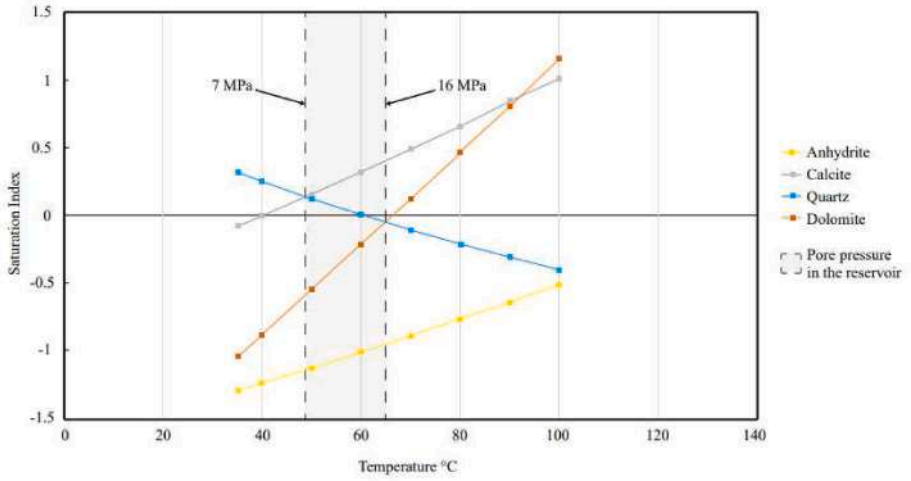

Fig. 15. Modeling of the SI, hydrostatic pressure and temperature of some solutes identified in the groundwater of the El Bañito thermal spring.

and gypsum cores from drilling in the Campeche Basin. These authors conclude that such high values, similar to those of current seawater, could be a consequence of closed basins with no connection or intermittent connection with global seawater. This would explain the high ratio of $^{87}Sr/^{86}Sr$ 0.70804 in the mLI, where the increase in organic matter indicates that the sediments were deposited in reducing and anoxic environments in a semi-enclosed basin. The same explanation could be considered for the middle part of the La Casita Formation, where the mEB with an $^{87}Sr/^{86}Sr$ ratio of 0.70847 occurs in calcareous shales interspersed with carboniferous shales; or for deeper and older evaporitic rocks with abundant gypsum, anhydrite and halite. Some springs with high concentrations of Sr and $^{87}Sr/^{86}Sr$ are located in intersections of faults that can bring Sr to the surface through a hydraulically connected part in aquifers (Shoedarto et al., 2021). Detailed isotopic studies in the rocks of this basin are necessary to better understand the behavior of their relationships in the springs of the SCScp. This is consistent with González-Sánchez et al. (2007) where they highlight that the strata-bound deposits identified as belonging to the Mississippi Valley type in northeastern México, have a simple mineralogy. They are are generally monomineral deposits of celestite, barite,

Table 7
Selected geothermometers for the El Bañito thermal spring, obtained with the GeoSol software.

Geothermometer	Calibration	Temperature (°C)	Equations (to obtain temperature in °C)
Quartz	Verma and Santoyo (1997) (20 °C > T < 210 °C)	60 ± 4	$-\{44.119(\pm0.438)\} + \{0.24469(\pm0.00573)\} S - \{1.7414 \times 10-4 (\pm1.365 \times 10-5)\} S2 + \{79.305(\pm0.427)\} \log S$
Quartz	Fournier (1977) (without vapor loss)	60	$[1309/(5.19-\log S)]-273.15$

fluorite, and Zn–Pb ± barite, with gangue minerals, such as secondary gypsum, calcite, clays, and uranium minerals in subordinate amounts, most of them identified in the mineralogical speciation recorded in this study.

Geochemical modeling, geothermometers, and geology indicate that the geothermal reservoir is located in a carbonate-evaporite succession at a depth ranging between 800 m and 1700 m, with a maximum geostatic pressure of 38 MPa, a hydrostatic pressure between 7 MPa and 16 MPa, and a temperature between 49 °C and 67 °C. The El Baño de San Ignacio geothermal system in the municipality of Linares, Nuevo León, 100 km southeast of the SGBEEB also has an origin in carbonate-evaporite rocks, at a depth of less than 2000 m with respect to the surface (Garza-Castillo, 2006). Unfortunately, the San Ignacio geothermal system does not have isotopic information that allows for a better correlation between both systems. The same lack of isotopic data occurs for the hot springs that emerge along the front of the mountain range, such as Taninul, Ojo Caliente, and El Termal among others. Evaluation of these springs could shed more details regarding their genesis and characteristics of their reservoirs, to differentiate them in terms of their origin in a sedimentary basin, as in the case of the mEB, or possibly associated with late Cenozoic intraplate-type volcanism (Aranda-Gómez et al., 2005).

7. Conclusions

This assessment and the results have established that the concentration and type of solutes of the types of springs vary depending on the type of geological formation through which they circulate. They are mainly of the HCO_3 type in the "more calcareous" formations, and variable SO_4 where there is certain contribution of terrigenous material. Geochemical modeling, geothermometers and geology let us infer that the geothermal reservoir of the **SGBEEB** is located in a carbonate evaporite succession at a depth ranging between 800 m and 1700 m, with a maximum geostatic pressure of 38 MPa, a hydrostatic pressure between 7 and 16 MPa, and a temperature between 49 °C and 67 °C. The SCScp is part of a very efficient system to recharge the regional aquifer, but this condition also implies that the existence of sources of anthropogenic contamination may reach the water-bearing zones with similar migration velocities. The government of the State of Nuevo de Nuevo León (2020) has determined within its 2050 masterplan, that population growth will demand greater surface and groundwater resource extraction in the MMA, including expansion of the shallow and deep aquifer production well network. Careful planning to protect recharge zones both in terms of promoting a balance of infiltration and aquifer withdrawal are necessary to protect this valuable ecosystem.

CRediT authorship contribution statement

Jerjes Rigoberto Pantoja-Irys: Writing – original draft, Validation, Supervision, Software, Project administration, Investigation, Funding acquisition, Conceptualization. **Hugo Mujica-Sánchez:** Writing – review & editing, Visualization, Supervision, Methodology, Investigation, Funding acquisition, Data curation. **Luis Eduardo Arista-Cázares:** Writing – review & editing, Visualization, Software, Methodology,

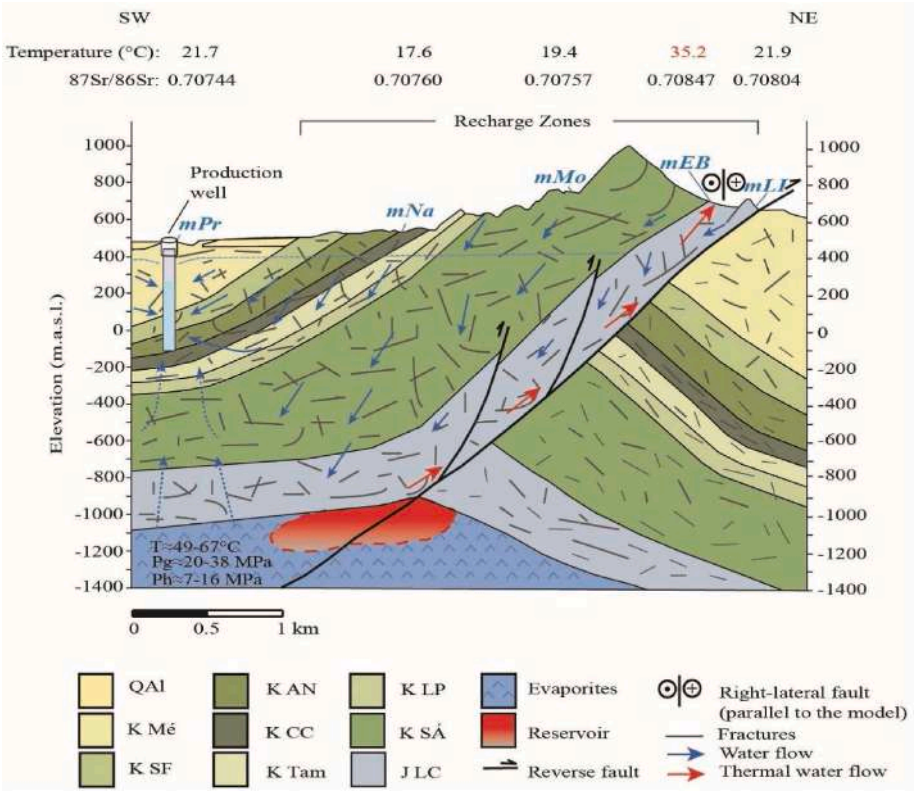

Fig. 16. Hydrogeological conceptual model of the SCScp.

Investigation, Formal analysis. **César Michel Hernández-García:** Visualization, Validation, Software, Methodology, Investigation, Formal analysis, Data curation. **Mark Wagner:** Writing – review & editing, Validation, Supervision, Resources, Methodology, Investigation, Formal analysis, Data curation, Conceptualization.

Declaration of competing interest

The authors declare the following financial interests/personal relationships which may be considered as potential competing interests:

Data availability

Data will be made available on request.

Acknowledgments

The research was funded by Corporación Ambiental de México S.A. de C.V. (CAM), as part of its training program for young earth science students. Special thanks to Ms Yadira Zulema Antonio-Durán who helped preparing Figs. 1 and 4 and with field support. We are very grateful to the professors of the Facultad de Ciencias de La Tierra, Universidad Autónoma de Nuevo León who supported the implementation of this investigation program. The authors sincerely thank CAM's staff, who shared its technical knowledge with the authors of this study. We are very grateful for the critical comments of Dr. Yam Zul Ernesto Ocampo-Díaz and an anonymous reviewer who greatly improved this contribution.

References

Adatte, T., Stinnesbeck, W., Remane, J., Hubberten, H., 1996. Paleoceanographic changes at the jurassic-cretaceous boundary in the western Tethys, northeast Mexico. Cretac. Res. 17, 671–689. https://doi.org/10.1006/cres.1996.0036.

Aguilar Vásquez, Y., 2003. Clasificación de la vegetación de la sierra Cerro de La Silla mediante una imagen de satélite y un análisis de factores abióticos. Master Thesis. Instituto Tecnológico de Monterrey, Monterrey, MX, p. 71.

Aguilar-Barajas, I., Sisto, P.N., Ramírez-Orozco, A.I., 2021. Agua para Monterrey. Logros, retos y oportunidades para Nuevo León y México. Instituto Tecnológico y de Estudios Superiores de Monterrey, p. 234.

Aguilar-Ramírez, C.F., Camprubí, A., Fitz-Díaz, E., Cienfuegos-Alvarado, E., Morales-Puente, P., 2017. Variación en la composición isotópica del agua meteórica a lo largo de la sección centro-noreste de la Sierra Madre Oriental. Bol. Soc. Geol. Mex. 69 (2), 447–463.

Alaníz-Alvarez, S.A., van der Heyden, P., Samaniego, A.F.N., Ortega-Gutiérrez, F., 1996. Radiometric and kinematic evidence for Middle Jurassic strike-slip faulting in southern Mexico related to the opening of the Gulf of Mexico. Geology 24, 443–446. https://doi.org/10.1130/0091-7613(1996)024.

Albert, J.F., Corominas, J., Paris, C., 1979. Estudio hidrogeológico de los manantiales y su aplicación geológica: caso de las aguas termales, carbónicas, y sulfhídricas de Cataluña. Acta Geol. Hisp.: Homenaje a Luis Solé í Sabarís 391–394.

Aranda-Gómez, J.J., Luhr, J.F., Housh, T.B., Valdez-Moreno, G., Chávez-Cabello, G., 2005. El volcanismo tipo intraplaca del Cenozoico tardío en el centro y norte de México: una revisión. Bol. Soc. Geol. Mex. 57 (3), 187–225. https://doi.org/10.18268/bsgm2005v57n3a1.

Barboza-Gudiño, J.R., Orozco-Esquivel, M.T., Gómez-Anguiano, M., Zavala-Monsiváis, A., 2008. The Early Mesozoic volcanic arc of western North America in northeastern Mexico. J. South Am. Earth Sci. 25, 49–63. https://doi.org/10.1016/j.jsames.2007.08.003.

Barboza-Gudiño Rafael, José, Ocampo-Díaz Zul Ernesto, Yam, Martínez, E, Loyola-Martínez, E, Pérez-Casillas G, I, et al., 2015. The Huizachal group in northeastern Mexico: a back-arc succession related to evolution of the early Jurassic Nazas arc Cordilleran section. Geological Society of America 11th Annual Meeting, Alaska, Geological Society of America 47 (4), 55–55.

Barboza-Gudiño, J.R., Ocampo-Díaz, Y.Z.E., Zavala-Monsiváis, A., López-Doncel, R.A., 2014. Procedencia como herramienta para subdivisión estratigráfica del Mesozoico temprano en el noreste de México. Rev. Mex. Ciencias Geol. 31 (3), 303–324.

Bassett, K., Busby, C., 2005. Tectonic setting of the glance conglomerate along the Sawmill canyon fault zone, southern Arizona: a sequence analysis of an intra-arc strike-slip basin. In: Anderson, T.H., Nourse, J.A., McKee, J.W., Steiner, M.B. (Eds.), The Mojave-Sonora Megashear Hypothesis: Development, Assessment, and Alternatives 393. Geological Society of America, Special Paper, pp. 377–400.

Billarent-Cedillo, A., Levresse, G., Ferrari, L., Inguaggiato, C., Inguaggiato, S., Hernández-Pérez, E., Hernández-Espriú, A., Corbo-Camargo, F., Carrera-Hernández, J., Arias-Paz, A., 2021. Deciphering origins and pathways of low-enthalpy geothermal waters in the unconventional geothermal system of Juchipila graben (Central Mexico). Geothermics 94, 1–14.

Blasco, M., Auqué, L.F., Gimeno, M.J., Acero, P., Asta, M.P., 2017. Geochemistry, geothermometry and influence of the concentration of mobile elements in the chemical characteristics of carbonate-evaporitic thermal systems. The case of the Tiermas geothermal system (Spain). Chem. Geol. 466, 696–709.

Blasco, M., Gimeno, M.J., Auqué, L.F., 2018. Low temperature geothermal systems in carbonate-evaporitic rocks: mineral equilibria assumptions and geothermometrical calculations. Insights from the Arnedillo thermal waters (Spain). Sci. Total Environ. 615, 526–539.

Blasco, M., Auqué, L.F., Gimeno, M.J., Acero, P., Gómez, J., Asta, M.P., 2019. Mineral equilibria and thermodynamic uncertainties in the geothermometrical characterization of carbonate geothermal systems of low temperature. The case of the Alhama-Jaraba system (Spain). Geothermics 78, 170–182. https://doi.org/10.1016/j.geothermics.2018.11.004.

Boschman, L., Molina-Garza, R.S., Langereis, C.G., van Hinsbergen, D.J.J., 2018. Paleomagnetic constraints on the kinematic relationship between the Guerrero terrane (Mexico) and North America since Early Cretaceous time. Geol. Soc. Am. Bull. 130 (7–8), 1131–1142. https://doi.org/10.1130/B31916.1.

Busby, C., 2012. Extensional and transtensional continental arc basins: case studies from the southwestern United States. In: Busby, C., Azor, A. (Eds.), Tectonics of Sedimentary Basins: Recent Advances. Wiley-Blacwell, pp. 382–404.

Centeno-García, E., 2017. Mesozoic tectono-magmatic evolution of Mexico: an overview. Ore Geol. Rev. 81, 1035–1052. https://doi.org/10.1016/j.oregeorev.2016.10.010.

Chiodini, G., Frondini, F., Marini, L., 1995. Theoretical geothermometers and PCO2 indicators for aqueous solutions coming from hydrothermal systems of medium-low temperature hosted in carbonate-evaporite rocks. Application to the thermal springs of the Etruscan Swell. Italy. Applied Geochemistry 10, 337–346.

Comisión Nacional del Agua (CONAGUA), 2020. Actualización de la disponibilidad media anual de agua en el acuífero cañon del Huajuco (1911). Ciudad de México, p. 29. Technical report. https://sigagis.conagua.gob.mx/gas1/Edos_Acuiferos_18/nleon/DR_1911.pdf. consultation: 3 de August de 2021.

Daniilidis, A., Herber, R., 2017. Salt intrusions providing a new geothermal exploration target for higher energy recovery at shallower depths. Energy 118, 658–670. https://doi.org/10.1016/j.energy.2016.10.094.

de Nuevo León, Gobierno, 2020. Plan maestro para garantizar el Agua de Nuevo León hasta el 2050, p. 41.

Dickinson, W.R., Lawton, T.F., 2001. Carboniferous to Cretaceous assembly and fragmentation of Mexico. Geol. Soc. Am. Bull. 113 (9), 1142–1160. https://doi.org/10.1130/0016-7606(2001)1132.0.CO;2.

Dunham, R.J., 1962. Classification of carbonate rocks according to depositional texture. In: Ham, W.E. (Ed.), Classification of Carbonate Rocks. AAPG, Tulsa, OK, pp. 108–121.

Edmunds, W.M., Smedley, P.L., 2000. Residence time indicators in groundwater: the East Midlands Triassic sandstone aquifer. Appl. Geochem. 15, 737–752. https://doi.org/10.1016/S0883-2927(99)00079-7.

Eguiluz de Antuñano, S., 1991. Interpretación geológica y geofísica de la Curvatura de Monterrey, en el noreste de México. Revista Ingeniería Petrolera 31, 25–39.

Eguiluz de Antuñano, S., 2001. Geologic evolution and gas resources of the sabinas basin in northeastern Mexico. In: Bartolini, C., Buffler, R.T., Cantú-Chapa, A. (Eds.), The Western Gulf of Mexico Basin Tectonics: Sedimentary Basins, and Petroleum Systems, vol. 75. The American Association of Petroleum Geologists Memoir, Tulsa, OK, pp. 241–270. https://doi.org/10.1306/M75768C10.

Ellis, A.J., 1959. The solubility of calcite in carbon dioxide solutions. Am. J. Sci. 257 (5), 354–365. https://doi.org/10.2475/ajs.257.5.354.

Espinasa-Pereña, R., Nieto-Torres, A., 2015. Análisis de la vulnerabilidad a fenómenos kársticos: México, Technical Report. Secretaría de Gobernación, Coordinación Nacional de Protección Civil, Centro Nacional de Prevención de Desastres, p. 41.

Fastovsky, D.E., Hermes, O.D., Strater, N.H., Bowring, S.A., Clark, J.M., Montellano, M., Hernández, R., 2005. Pre-Late Jurassic, fossil-bearing volcanic and sedimentary red beds of Huizachal canyon, Tamaulipas, Mexico. In: Anderson, T.H., Nourse, J.A., Mckee, J.W., Steiner, M.B. (Eds.), The Mojave-Sonora Megashear Hypothesis: Development, Assessment, and Alternatives 393. Geological Society of America, Special Paper, pp. 401–426. https://doi.org/10.1130/0-8137-2393-0.401.

Fillon, R.H., 2007. Mesozoic Gulf of Mexico basin evolution from a planetary perspective and petroleum system implications. Petrol. Geosci. 13, 105–126. .https://doi.org/10.1144/1354-079307-745.

Fish, J.E., 1977. Karst Hydrogeology and Geomorphology of the Sierra de El Abra and the Valles-San Luis Potosí Region, México. PhD Thesis. McMaster University, Hamilton, CA, p. 469.

Fitz-Díaz, E., Lawton, T.F., Juárez-Arriaga, E., Chávez-Cabello, G., 2018. The Cretaceous-Paleogene Mexican orogen: structure, basin development, magmatism and tectonic. Earth Sci. Rev. 183, 56–84. https://doi.org/10.1016/j.earscirev.2017.03.002.

Folk, R.L., 1962. Spectral subdivision of limestone types. In: Ham, W.E. (Ed.), Classification of Carbonate Rocks, vol. 1. American Association of Petroleum Geologists, Memoir, pp. 62–84.

Fournier, R.O., 1977. Chemical geothermometers and mixing models for geothermal systems. Geothermics 5, 41–50.

Gamper, M.A., 1977. Estratigrafía y Microfacies Cretácicas del Anticlinorio Huizachal-Peregrina (Sierra Madre Oriental). Bol. Soc. Geol. Mex. 38 (2), 1–17. https://doi.org/10.18268/bsgm1977v38n2a1.

García-Díaz, J.L., 2004. Etude Géologique de la Sierra Madre del sur aux environs de Chilpancingo et D'Olinala, Gro: Une contribution à la connaissance de l'évolution géodynamique de la marge pacifique du Mexique depuis le Jurassique. Ph.D Thesis. Université de Savoie, Chambery, p. 148.

Garza-Castillo, A.M., 2006. Caracterización hidrogeoquímica de las aguas termales del Baño San Ignacio, Linares, Nuevo León, México. Master Thesis. Universidad Autónoma de Nuevo León, Linares, MX, p. 96.

Giggenbach, W.F., 1988. Geothermal solute equilibria. Derivation of Na-K-Mg-Ca geoindicators. Geochem. Cosmochim. Acta 52 (12), 2749–2765. https://doi.org/10.1016/0016-7037(88)90143-3.
Giggenbach, W.F., 1992. Isotopic shifts in waters from geothermal and volcanic systems along convergent plate boundaries and their origin. Earth Planet Sci. Lett. 113 (4), 495–510. https://doi.org/10.1016/0012-821X(92)90127-H.
Gill, R., 2015. Chemical Fundamentals of Geology and Environmental Geoscience. WILEY-Blackwell, London, UK, p. 288.
Giordano, M., 2009. Global groundwater? Issues and solutions. Annu. Rev. Environ. Resour. 34, 153–178. https://doi.org/10.1146/annurev.environ.030308.100251.
Godínez-Urban, A., Lawton, T.F., Molina-Garza, R.S., Iriondo, A., Weber, B., López-Martínez, M., 2011. Jurassic volcanic and sedimentary rocks ofthe La Silla and Todos Santos Formations, Chiapas: record of Nazas arc magmatism and rift-basin formation prior to opening of the Gulf of Mexico. Geosphere 7, 121–144.
Goldhammer, R.K., 1999. Mesozoic sequence stratigraphy and paleogeographic evolution, Northeast Mexico. In: Bartolini, C., Wilson, J.L., Lawton, T.F. (Eds.), Mesozoic Sedimentary and Tectonic History of North-Central Mexico, vol. 340. Geological Society of America Special Paper, pp. 1–58.
Goldhammer, R.K., Johnson, A.C., 2001. Middle jurassic-upper cretaceous paleogeographic evolution and sequence-stratigraphic framework of the northwest Gulf of Mexico rim. In: Bartolini, C., Buffler, R.T., Cantú-Chapa, A. (Eds.), The Western Gulf of Mexico Basin Tectonics: Sedimentary Basins, and Petroleum Systems, vol. 75. The American Association of Petroleum Geologists Memoir, Tulsa, OK, pp. 45–82. https://doi.org/10.1306/M75768C3.
González, P.A., y Sosa, C.M., 2003. Análisis de la vegetación del área de protección de flora y fauna Cañón de Santa Elena (desierto chihuahuense, México) utilizado Modelos Digitales de Elevación. Ecosistemas 12 (2), 1–6.
González-Sánchez, F., Puente-Solís, R., González-Partida, E., Camprubí, A., 2007. Estratigrafía del Noreste de México y su relación con los yacimientos estratoligados de fluorita, barita, celestina y Zn-Pb. Bol. Soc. Geol. Mex. 59 (1), 43–62.
Gray, G.G., Pottorf, R.J., Yurewicz, D.A., Mahon, K.I., Pevear, D.R., Chuchla, R.J., 2001. Thermal and chronological record of syn- to post-laramide burial and exhumation. In: Bartolini, C., Buffler, R.T., Cantú-Chapa, A. (Eds.), The Western Gulf of Mexico Basin Tectonics: Sedimentary Basins, and Petroleum Systems, vol. 75. The American Association of Petroleum Geologists Memoir, Tulsa, OK, pp. 159–181. https://doi.org/10.1306/M75768C7.
Haenggi, W.T., 2002. Tectonic history of the chihuahua trough, Mexico and adjacent USA, part II: mesozoic and cenozoic. Bol. Soc. Geol. Mex. 55 (1), 38–94.
Imlay, R.W., 1936. Evolution of the Coahuila Peninsula, Mexico, part IV, geology of the western part of the Sierra de Parras. GSA Bull. 47 (7), 1091–1152.
Instituto Nacional de Estadística y Geografía (INEGI), 2012. Digital Elevation Model, LIDAR, Escale 1:10,000., Format GRID. Maps: G14C36B1; G14C36B2; G14C36B3; G14C36B4; G14C36C; G14C36C3.
Instituto Nacional de Estadística y Geografía (INEGI), 2020. Censo Nacional de Población y Vivienda.
Jordana, S., Gurguí, A., Batista, E., 2009. Hidráulica de Acuíferos. In: Comisión Docente Curso Internacional de Hidrología Subterránea. Hidrogeología. Conceptos básicos de hidrología subterránea. Fundación Centro Internacional de Hidrología Subterránea, Barcelona, pp. 184–313.
Khan, M.I., Islam, M.R., 2007. Reservoir engineering and secondary recovery. In: Khan, M.I., Islam, M.R. (Eds.), The Petroleum Engineering Handbook: Sustainable Operations, pp. 189–241. https://doi.org/10.1016/B978-1-933762-12-8.50013-1.
Lawton, T.F., Molina-Garza, R.S., 2014. U-Pb geochronology of the type Nazas Formation and superjacent strata, northeastern Durango, Mexico: implication of a Jurassic age for continental-arc magmatism in north-central Mexico. Geol. Soc. Am. Bull. 126 (10), 1181–1199. https://doi.org/10.1130/B30827.1.
Lehmann, C., Osleger, D.A., Montañez, I.P., Sliter, W., Arnaud-Vanneau, A., Banner, J.L., 1999. Evolution of Cupido and Coahuila carbonate platforms, early cretaceous, northeastern Mexico. Geol. Soc. Am. Bull. 111 (7), 1010–1029.
Longoria, J.F., 1975. Estratigrafía de la serie Comancheana del noreste de México. Bol. Soc. Geol. Mex. 36 (1), 31–59. https://doi.org/10.18268/bsgm1975v36n1a2.
Longoria, J.F., 1984. Stratigraphic studies in the jurassic of northeastern Mexico: evidence for the origin of the sabinas basin. In: Ventress, W.P.S., Bebout, D.G., Perkins, B.F., Clyde, H., Moore, C.H. (Eds.), The Jurassic of the Gulf Rim: Gulf Coast Section of the Society for Sedimentary Geology. GCSSEPM Foundation, pp. 171–193. https://doi.org/10.5724/gcs.84.03.0171.
Longoria, J.F., 1998. The mesozoic of the Mexican cordillera in Nuevo leon, NE Mexico. In: Longoria, J.F., Krutak, P.R., Gamper, M.A. (Eds.), Geologic Studies in Nuevo León, Mexico. Sociedad Mexicana de Paleontología, Special Publication, pp. 1–44.
Longoria, J.F., Dávila, V.M., 1979. Estratigrafía y microfacies del Cerro de La Silla, SE de Monterrey. Boletín del Departamento de Geología de la Universidad de Sonora 2 (1), 65–95.
Lugo Hubp, J., 1990. El relieve de la República mexicana. Rev. Institut. Geol. 9 (1), 82–111.
Martínez-Paco, M., Velasco-Tapia, F., Santana-Salas, L.A., Juárez-Arriaga, E., Aceves de Alba, J., Ocampo-Díaz, Y.Z.E., 2022. San Felipe and Caracol tuffaceous sandstones, NE Mexico – late Cretaceous continental arc petrogenetic link: petrographic, geochemical, and geochronological evidence. J. S. Am. Earth Sci. 116, 1–24. https://doi.org/10.1016/j.jsames.2022.103818.
Marton, G.L., 1995. Jurassic Evolution of the Southeastern Gulf of Mexico. PhD Thesis. The University of Texas, Austin, TX, p. 276.
Michalzik, D., Schumann, D., 1994. Lithofacies relations and paleoecology of a Late Jurassic to Early Cretaceous fan delta to shelf depositional system in the Sierra Madre Oriental of north-east Mexico. Sedimentology 41 (3), 463–477. https://doi.org/10.1111/j.1365-3091.1994.tb02006.x.
Molina-Garza, R.S., Van Der Voo, R.O.B., Urrutia-Fucugauchi, J., 1992. Paleomagnetism of the Chiapas Massif, southern Mexico: evidence for rotation of the maya block and implications for the opening of the Gulf of Mexico. Geol. Soc. Am. Bull. 104, 1156–1168. https://doi.org/10.1130/0016-7606(1992)1042.3. CO;2.
Montanari, D., Minissale, A., Doveri, M., Gola, G., Trumpy, E., Santilano, A., Manzella, A., 2017. Geothermal resources within carbonate reservoirs in western Sicily (Italy): a review. Earth Sci. Rev. 169, 180–201. https://doi.org/10.1016/j.earscirev.2017.04.016.
Mora, A., Mahlknecht, J., Rosales-Lagarde, L., Hernández-Antonio, A., 2017. Assessment of major ions and trace elements in groundwater supplied to the Monterrey metropolitan area, Nuevo León, Mexico. Environ. Monit. Assess. 189 (394), 1–15. https://doi.org/10.1007/s10661-017-6096-y.
Muir, J.M., 1934. Limestone reservoir rocks in the Mexican oil fields. In: Wrather, W.E., Lahee, F.H. (Eds.), Problems of Petroleum Geology. American Association of Petroleum Geologists, Tulsa, OK, pp. 377–398.
Muir, J.M., 1936. Geology of the Tampico Region. México. American Association of Petroleum Geologists, Tulsa, OK, p. 280.
Noack, C.W., Dzombak, D.A., Karamalidis, A.K., 2014. Rare earth element distributions and trends in natural waters with a focus on groundwater. Environ. Sci. Technol. 48 (8), 4317–4326. https://doi.org/10.1021/es4053895.
Ocampo-Díaz, Y.Z.E., 2011. Implicaciones tectono-sedimentarias de las intercalaciones clásticas en el límite Jurásico-Cretácico del Noreste de México (Fosa de Monterrey y Cuenca de Sabinas). Ph.D.Thesis. Universidad Autónoma de Nuevo León, Linares, MX, p. 275.
Ocampo-Díaz, Y.Z.E., Rubio Cisneros, I.I., 2013. Reciclamiento sedimentario: análisis composicional asociado a discordancias del noroeste de México, un ejemplo del Triásico Superior al Cretácico Inferior. Bol. Soc. Geol. Mex. 65, 553–572.
Ocampo-Díaz, Y.Z.E., Talavera-Mendoza, O., Jenchen, U., Valencia, V.A., Medina-Ferrusquia, H.C., Guerrero-Suastegui, M., 2014. Procedencia de la Formación La Casita y la Arcosa Patula: implicaciones para la evolución tectono-magmática del NE de México entre el Carbonífero y el Jurásico. Rev. Mex. Ciencias Geol. 31, 45–63.
Ocampo-Díaz, Y.Z.E., Pinzón-Sotelo, M.P., Chávez-Cabello, G., Ramírez-Díaz, A., Martínez-Paco, M., Velasco-Tapia, F., Guerrero-Suastegui, M., Barboza- Gudiño, J.R., 2016. Propuesta nomenclatural y análisis de procedencia de la Formación Concepción del Oro (antes Formación Caracol): implicaciones sobre la evolución tectónica del sur de Norteamérica durante el Cretácico Tardío. Rev. Mex. Ciencias Geol. 33 (1), 3–33.
Ocampo-Díaz, Y.Z.E., Torres-Sánchez, S.A., Augustsson, C., Barboza-Gudiño, J.R., García-Díaz, J.L., Talavera-Mendoza, O., Aceves de Alba, J., Castro-Larragoitia, G.J., Martínez-Paco, M., Saucedo, R., Aguillón-Robles, A., 2019. Provenance and tectonic setting of the jurassic Huayacocotla Formation and alamitos sandstone, Central Mexico. Geochem. 79, 369–383. https://doi.org/10.1016/j.chemer.2019.05.004.
Ocampo-Díaz, Y.Z.E., Augustsson, C., Guerrero-Suastegui, M., Aceves de Alba, J., Barboza-Gudiño, J.R., Martínez-Paco, M., Torres-Sánchez, S.A., 2022. A wave to tidal influenced deltaic coastline in a carbonate environment: the Late Jurassic to Early Cretaceous La Casita Formation, northeastern México. J. S. Am. Earth Sci. 115, 1–20.
Olivares-Ramos, D., 2006. Zonación de calpionélidos y análisis microfacial de la transición Tithoniano – Berriasiano, sierra de La Silla, Nuevo León, México. Bachelor Thesis. Universidad Autónoma de Nuevo León, Linares, p. 89.
Onajite, E., 2017. Practical Solutions to Integrated Oil and Gas Reservoir Analysis. Geophysical and Geological Perspectives. Elsevier Inc., New York, p. 452.
Parkhurst, D.L., Appelo, C.A.J., 2013. Description of input and examples for PHREEQC (version 3) - a computer program for speciation, batch-reaction, one-dimensional transport, and inverse geochemical calculations. United States Geological Survey Techniques and Methods 6 (A43), 497. http://pubs.usgs.gov/tm/06/a43.
Pindell, J., 1985. Alleghenian reconstruction and subsequent evolution of the Gulf of Mexico, Bahamas, and Proto-Caribbean. Tectonics 4 (1), 1–3. https://doi.org/10.1029/TC004i001p00001.
Pindell, J., Kennan, L., 2009. Tectonic evolution of the Gulf of Mexico, Caribbean and northern South America in the mantle reference frame: an update. In: James, K.H., Lorente, M.A., Pindell, J.L. (Eds.), The Origin and Evolution of the Caribbean Plate 328. Geological Society of London, London, Special Publication, pp. 1–55. https://doi.org/10.1144/SP328.1.
Pindell, J., Weber, B., Hale-Erlich, W., Cossey, S., Bitter, M., Molina Garza, R., Graham, R., Erlich, R.N., 2020. Strontium isotope dating of evaporites and the breakup of the Gulf of México and proto–caribbean seaway. In: Martens, U., Molina Garza, R.S. (Eds.), Southern and Central México: Basement Framework, Tectonic Evolution, and Provenance of Mesozoic–Cenozoic Basins, vol. 546. Geological Society of America Special Paper, pp. 1–22. https://doi.org/10.1130/2020.2546(12).
Prol-Ledesma, R.M., Morán Zenteno, D.J., 2019. Heat flow and geothermal provinces in México. Geothermics 78, 183–200. https://doi.org/10.1016/j.geothermics.2018.12.009.
Rohde, M.M., Froend, R., Howard, J., 2017. A global synthesis of managing groundwater dependent ecosystems under sustainable groundwater policy. Groundwater 55 (3), 293–301. https://doi.org/10.1111/gwat.12511.
Romo-Ramírez, J.R., Muñoz-Jarillo, C.R., Badillo-Cadena, L.A., Rodríguez-Medrano, D., 2021. Mining-geological Map Allende G14-C36, Scale 1:50,000. Servicio Geológico Mexicano, Hidalgo.
Rosaz, T., 1989. Les passage des Cordilléres Nord-Américaines aux Sierras Madres Mexicaines le long du Texas Lineament Géologie du SW du Nouveau-Mexique (USA). Bulletin des Centre de Recherches Exploration-Production Elf-Aquitaine 13 (2), 247–275.
Rubio-Cisneros, I.I., Lawton, T.F., 2011. Detrital zircon U-Pb ages of sandstones in continental red beds at Valle de Huizachal, Tamaulipas, NE Mexico: record of Early-

Middle Jurassic arc volcanism and transition to crustal extension. Geosphere 7 (1), 1–12. https://doi.org/10.1130/GES00567.1.

Secretaria de Medio Ambiente y Recursos Naturales (SEMARNAT), 2010. Norma Oficial Mexicana NOM-059-SEMARNAT-2010: Protección ambiental-Especies nativas de México de flora y fauna silvestres-Categorías de riesgo y especificaciones para su inclusión, exclusión o cambio-Lista de especies en riesgo. https://www.dof.gob.mx/normasOficiales/4254/semarnat/semarnat.htm.

Servicio Meteorológico Nacional (SMN), 2021. Estaciones Meteorológicas Automáticas (EMAS). https://smn.conagua.gob.mx/es/observando-el-tiempo/estaciones-meteorologicas-automaticas-ema-s.

Shoedarto, R.M., Tada, Y., Kashiwaya, K., Koike, K., Iskandar, I., Malik, D., Bratakusuma, B., 2021. Investigation of meteoric water and parent fluid mixing in a two-phase geothermal reservoir system using strontium isotope analysis: a case study from Southern Bandung, West Java, Indonesia. Geothermics 94, 1–15. https://doi.org/10.1016/j.geothermics.2021.102096.

Tardy, M., Longoria, J.F., Martínez-Reyes, J., Mitre-Salazar, L.M., Patiño, M., Padilla y Sánchez, R., Ramírez, C., 1975. Observaciones generales sobre la estructura de la Sierra Madre Oriental: la aloctonía del conjunto cadena alta-altiplano central, entre Torreón, Coah. y San Luis Potosí, S.L.P., vol. 1. Revista Instituto de Geología, México, pp. 1–11.

Velasco-Tapia, F., Martínez-Paco, M., Iriondo, A., Ocampo-Díaz, E.Z.Y., Cruz-Gámez, E. M., Ramos-Ledezma, A., Andaverde, J.A., Ostrooumov, M., Masuch, D., 2016. Altered volcanic ash layers of the late cretaceous san Felipe Formation, sierra Madre oriental (northeastern México): U-Pb geochronology, provenance and tectonic setting. J. S. Am. Earth Sci. 70, 18–35. https://doi.org/10.1016/j.jsames.2016.04.010.

Venegas-Rodríguez, G., Barboza-Gudiño, J.R., López-Doncel, R.A., 2009. Geocronología de circones detríticos en capas del Jurásico Inferior de las áreas de la Sierra de Catorce y el Alamito en el estado de San Luis Potosí. Rev. Mex. Ciencias Geol. 26, 466–481.

Verma, S.P., Santoyo, E., 1997. New improved equations for Na/K, Na/Li and SiO2 geothermometers by outlier detection and rejection. J. Volcanol. Geoth. Res. 79, 9–23.

Verma, S.P., Pandarinath, K., Santoyo, E., 2008. SolGeo: a new computer program for solute geothermometers and its applications to Mexican geothermal fields. Geothermics 37 (6), 597–621. https://doi.org/10.1016/j.geothermics.2008.07.004.

Verma, S.P., Uscanga-Junco, O.A., Díaz González, L., 2021. A statistically coherent robust multidimensional classification scheme for water. J. Sci. Teach. Educ. 750, 1–19. https://doi.org/10.1016/j.scitotenv.2020.141704.

Wassenaar, L.I., Van Wilgenburg, S.L., Larson, K., Hobson, K.A., 2009. A groundwater isoscape (δD, δ18O) for México. J. Geochem. Explor. 102 (3), 123–136. https://doi.org/10.1016/j.gexplo.2009.01.001.

White, T., Witzke, B., Ludvigson, G., Brenner, R., 2005. Distinguishing base-level change and climate signals in a Cretaceous alluvial sequence. Geology 33, 13–16. https://doi.org/10.1130/G20995.1.

Winker, C.D., Buffler, R.T., 1988. Paleogeographic evolution of early deep-water Gulf of Mexico and margins, jurassic to middle cretaceous (comanchean). Am. Assoc. Petrol. Geol. Bull. 72, 318–346.

Wolaver, B.D., Crossey, L.J., Karlstrom, K.E., Banner, J.L., Cardenas, M.B., Gutiérrez-Ojeda, C., Sharp, J.M., 2013. Identifying origins of and pathways for spring waters in a semiarid basin using He, Sr, and C isotopes: cuatrociénegas Basin. México. Geosphere 9 (1), 11–125.

Yang, P., Dan, L., Groves, C., Xie, S., 2019. Geochemistry and genesis of geothermal well water from a carbonate–evaporite aquifer in Chongqing, SW China. Environ. Earth Sci. 33, 1–14. https://doi.org/10.1007/s12665-018-8004-3.

Zhang, J., 2013. Effective stress, porosity, velocity and abnormal pore pressure prediction accounting for compaction disequilibrium and unloading. Mar. Petrol. Geol. 45, 2–11. https://doi.org/10.1016/j.marpetgeo.2013.04.007.